BIOCHEMISTRY

BRK phosphorylates SMAD4 for proteasomal degradation and inhibits tumor suppressor FRK to control SNAIL, SLUG, and metastatic potential

S. Miah[1,2], C. A. S. Banks[1], Y. Ogunbolude[2], E. T. Bagu[2]*, J. M. Berg[2], A. Saraf[1], T. T. Tettey[1], G. Hattem[1], G. Dayebgadoh[1], C. G. Kempf[1], M. Sardiu[1], S. Napper[2,3], L. Florens[1], K. E. Lukong[2†], M. P. Washburn[1,4†]

The tumor-suppressing function of SMAD4 is frequently subverted during mammary tumorigenesis, leading to cancer growth, invasion, and metastasis. A long-standing concept is that SMAD4 is not regulated by phosphoryl ation but ubiquitination. Our search for signaling pathways regulated by breast tumor kinase (BRK), a nonreceptor protein tyrosine kinase that is up-regulated in ~80% of invasive ductal breast tumors, led us to find that BRK competitively binds and phosphorylates SMAD4 and regulates transforming growth factor–β/SMAD4 signaling pathway. A constitutively active BRK (BRK-Y447F) phosphorylates SMAD4, resulting in its recognition by the ubiquitin-proteasome system, which accelerates SMAD4 degradation. Activated BRK–mediated degradation of SMAD4 is associated with the repression of tumor suppressor gene *FRK* and increased expression of mesenchymal markers, SNAIL, and SLUG. Thus, our data suggest that combination therapies targeting activated BRK signaling may have synergized the benefits in the treatment of SMAD4 repressed cancers.

INTRODUCTION

Breast tumor kinase (BRK) is a nonreceptor tyrosine kinase highly expressed in most breast cancer cell lines and tumors (*1*). It displays a similar architecture and 30 to 40% sequence identity with Src family kinases. It is composed of an Src homology three domain (SH3 domain), an SH2 domain, and a catalytic tyrosine kinase domain. Similar to Src, BRK is negatively regulated by phosphorylation of its C-terminal tyrosine-447 and activated by phosphorylation of tyrosine-342 in the catalytic domain. Mutation of tyrosine-447 to phenylalanine substantially enhances the kinase activity of BRK (*2*).

BRK has been implicated in several signaling cascades, notably in mitogenic signaling (*3*). It has been shown to enhance the mitogenic signals of epidermal growth factor (EGF) by promoting the activation of Akt (*4*). Various EGF receptor ligands, including EGF and heregulin, have been shown to stimulate BRK activity, resulting in increased cell proliferation and migration (*4*–*6*). Consistent with this, BRK has been shown to promote human EGF receptor 2 (HER2)–induced tumorigenesis in orthotropic transplantation–based models (*7*). We have also reported that BRK activation significantly enhances tumor formation in xenograft models (*2*). In addition, BRK is overexpressed in over 80% of breast carcinomas (*1*) and in many other major cancer types including lung (*8*), ovarian (*9*), and pancreatic (*10*) cancers. Although the cellular role of BRK in carcinogenesis has been established, its role in controlling signal transduction pathways is still unclear.

Here, we first used a kinome array (*11*) to elucidate the role of BRK in regulating signal transduction pathways and identified components of the transforming growth factor–β (TGF-β)/SMAD signaling pathway as candidate BRK targets. Although the major molecular components of the TGF-β/SMAD signaling pathway are known, the dynamics of TGF-β/SMAD signaling remains unclear in many systems, including normal and cancer cells. Current evidence supports that upon TGF-β/bone morphogenetic protein receptor activation, SMAD2 and SMAD3 or SMAD1, SMAD5, and SMAD8 bind SMAD4 forming SMAD complexes, which translocate into the nucleus to initiate gene regulation (*12*, *13*). Although TGF-β/SMAD signaling networks have played pivotal roles in biological processes, disruption of their signaling has been implicated in several developmental disorders and diseases including cancers (*12*). The TGF-β signaling pathway can play contradictory roles during tumor development. It can function to suppress tumorigenesis, impeding the proliferation of transformed cells during the early stage of tumorigenesis (*12*, *14*). In contrast, in some advanced cancers, loss-of-function mutations or low expression of SMAD2, SMAD3, and SMAD4 have been observed leading to the suppression of the TGF-β signaling pathway (*12*, *15*) and uncontrolled cell proliferation (*14*). Moreover, SMAD2 and SMAD4 are being listed among the 127 most mutated genes in 12 major cancer types (*16*).

Given the complexity of TGF-β/SMAD signaling networks in biological processes, we set out to investigate how a nonreceptor tyrosine kinase such as BRK may regulate the function and network of the TGF-β/SMAD signaling pathway. We used complementary immunological, biochemical, genomics, and proteomics approaches to understand how BRK might regulate TGF-β/SMAD protein interaction networks and signal transduction pathways. Collectively, our results provide evidence that BRK regulates the TGF-β/SMAD signal transduction pathway in cancer and normal cells. BRK-mediated phosphorylated SMAD4 is targeted for proteasomal degradation, resulting in down-regulation of the tumor suppressor Fyn-related kinase (FRK) and up-regulation of the epithelial-mesenchymal transition (EMT) markers SNAIL and SLUG in cancer cells. Together,

[1]Stowers Institute for Medical Research, Kansas City, MO 64110, USA. [2]Department of Biochemistry, College of Medicine, University of Saskatchewan, Saskatoon, SK S7N 5E5, Canada. [3]Vaccine and Infectious Disease Organization–International Vaccine Centre, University of Saskatchewan, Saskatoon, SK S7 N 5E3, Canada. [4]Departments of Pathology and Laboratory Medicine, University of Kansas Medical Centre, Kansas City, KS 66160, USA.
*Present address: Division of Basic Biomedical Sciences, Sanford School of Medicine, The University of South Dakota, Vermillion, SD 57069, USA.
†Corresponding authors. Email: kiven.lukong@usuask.ca (K.E.L.); mpw@stowers.org (M.P.W.)

our work provides a rationale for therapeutically targeting BRK in patients with SMAD4-deficient cancer.

RESULTS

Components of the TGF-β/SMAD pathway are potential BRK targets

BRK is overexpressed in most breast cancer cell lines and tumors (*2*), and importantly, BRK is activated in the plasma membrane of human breast tumors (*17*). To substantiate the overexpression of BRK in most major cancer types, we interrogated the gene expression database, GENT (Gene Expression across Normal and Tumors; http://medicalgenome.kribb.re.kr/GENT/reference.php). We found that the expression of BRK mRNA was significantly higher ($P \leq 0.05$) in all five cancer types that we queried compared to their respective noncancerous tissues (Fig. 1A). Having confirmed that BRK overexpression is prevalent in cancers, we next sought to identify BRK targets.

In this study, we focused on the constitutively active form of BRK, BRK-Y447F (termed BRK-YF from here on). We have previously demonstrated that BRK-YF displayed higher kinase activity than BRK–wild-type (WT) when ectopically and stably expressed in human embryonic kidney (HEK) 293 cells (*2*). To decipher the role of activated BRK in cellular signal transduction

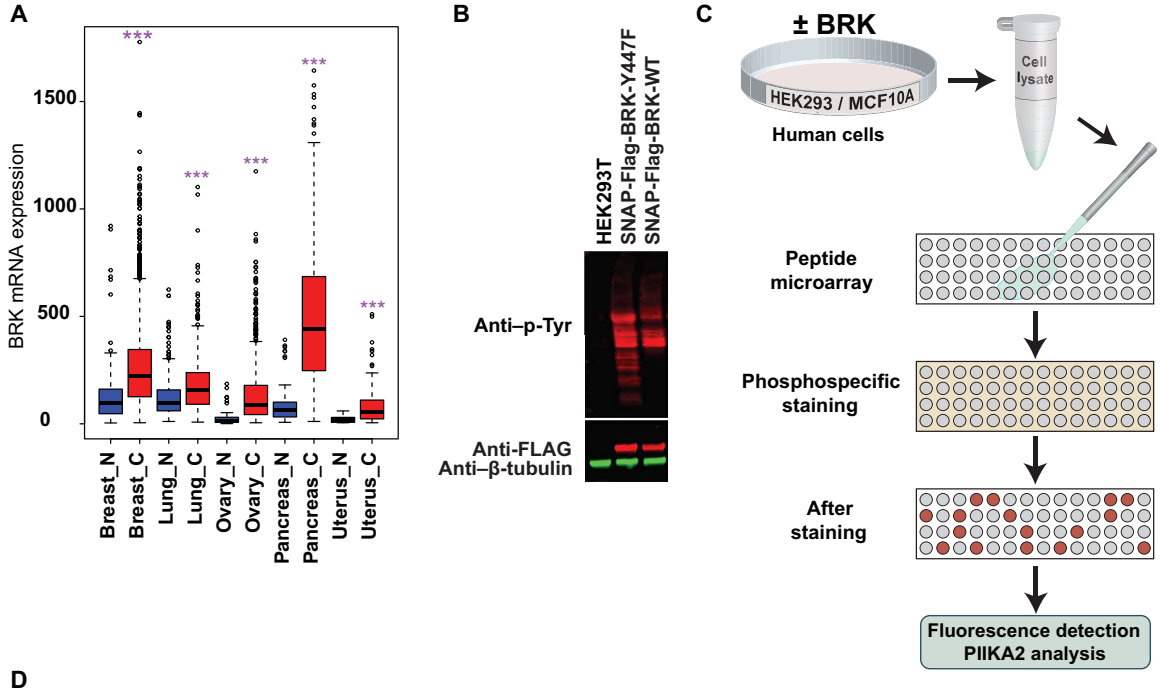

D

Source pathway	Pathways affected by BRK-YF in HEK 293 cells	*P* value	Targeted molecules in the signaling pathways
KEGG	TGF-β signaling pathway	0.012	RPS6KB1 ; SMAD2 ; SMAD3 ; TGFBR1 ; TGFBR2
PID BIOCARTA	TGF-β signaling pathway	0.012	SMAD2 ; SMAD3 ; TAB1 ; TGFBR1 ; TGFBR2 ;
PID NCI	TGF-β receptor signaling	0.030	CAV1 ; CTNNB1 ; PDPK1 ; RPS6KB1 ; SHC1 ; SMAD2 ; SMAD3 ; TGFBR1 ; TGFBR2
PID NCI	Endogenous TLR signaling	0.031	CHUK ; HSPD1 ; IRAK1 ; MYD88
INOH	Negative feedback regulation of TGF-β signaling pathway by R-smad degradation (canonical TGF-β signaling pathway)	0.031	SMAD2 ; SMAD3 ; TGFBR1 ; TGFBR2
REACTOME	Signaling by TGF-β	0.031	SMAD2 ; SMAD3 ; TGFBR1 ; TGFBR2

Fig. 1. BRK is overexpressed in several human tumors and regulate different signaling pathways in normal and cancer cells. (**A**) Differential expression of *BRK* in five major cancer types. Data obtained from The Cancer Genome Atlas database, median ± one quartile; ***$P < 0.001$. Tissue samples are denoted N for normal and C for cancer tissue. (**B**) Activity of BRK–wild-type (WT) and BRK-Y447F (BRK-YF) mutants in transfected human embryonic kidney (HEK) 293 cells. BRK-WT and BRK-YF were transfected in HEK293 cells, and cell lysates were subjected to immunoblot with antiphosphotyrosine antibody (PY20), and anti-BRK and anti–β-tubulin served as a loading control. (**C**) Flow diagram of peptide arrays for kinome analysis. (**D**) Signaling pathways significantly ($P < 0.05$) affected by activated BRK as identified by kinome analysis in HEK293.

pathways, we expressed SNAP-FLAG tagged BRK-WT (SF-BRK-WT) and BRK-YF (SF-BRK-YF) constructs in HEK293 cells and evaluated their global kinase activity by analyzing cell lysates by Western blotting. When we visualized phosphorylated proteins using the PY20 antiphosphotyrosine antibody, we confirmed that BRK-YF showed higher kinase activity than BRK-WT (Fig. 1B and fig. S1A).

Next, we used a kinome peptide array to identify potential signaling pathways regulated by activated BRK in BRK-YF–expressing stable cells. This well-characterized kinome array (*11*) consisted of 300 distinct target peptides corresponding to different signaling molecules involved in various signal transduction pathways, including the TGF-β/SMAD, mammalian target of rapamycin (mTOR) , phosphatidylinositol 3-kinase, integrin, Janus kinase–signal transducers and activators of transcription, and mitogen-activated protein kinase (MAPK) pathways. We analyzed lysates from stably expressing green fluorescent protein (GFP)–BRK-YF and parental MCF10A and HEK293 cells using this kinome platform (Fig. 1C). We observed that potential BRK targets were enriched for components of several signaling pathways, notably the TGF-β/SMAD signaling pathway ($P \leq 0.05$; Fig. 1D and fig. S1B).

SMAD4 is a cytosolic target of BRK

As our kinome array data suggested that SMAD family proteins were potential targets for BRK-mediated phosphorylation, we next asked whether SMAD2/3/4 interacted with BRK. First, we expressed Halo-SMAD2/3/4 either alone or with SF-BRK-YF into HEK293 cells, followed by affinity purification using magnetic beads against Halo and SNAP. We found that SF-BRK-YF copurified with either SMAD2, SMAD3, or SMAD4 (Fig. 2A). We also observed a reciprocal association when SF-BRK-YF was coexpressed with either Halo-SMAD2/3/4 or affinity purified with Halo magnetic beads (Fig. 2B). Since all three of the SMAD proteins (Halo-SMAD2/3/4) interacted with BRK-YF, we next determined which of them, if any, had the strongest interaction with BRK. We coexpressed Halo-SMAD2/3/4, together with SF-BRK-YF in HEK293 cells, and affinity purified proteins from the resulting whole-cell lysates with Halo magnetic beads. We then analyzed these proteins by immunoblotting with specific antibodies against SMAD2, SMAD3, and SMAD4. We detected SMAD4, but neither SMAD2 nor SMAD3 in the SF-BRK purified sample, suggesting that in the presence of all three SMAD proteins, SMAD4 competitively binds SF-BRK-YF, possibly indicating a stronger affinity of SMAD4 toward SF-BRK-YF (Fig. 2C).

Next, to map the domains of BRK important for interaction with SMAD4, we ectopically expressed five BRK mutants with GFP-SMAD4 in HEK293 cells. These included three mutants affecting the Src homology domains: BRK-W44A; ΔSH2-BRK, which lacks the SH2 domain; and ΔSH3-BRK, which lacks the SH3 domain. In addition, we used two mutants to assess whether BRK activity was necessary for interaction: the kinase-inactive BRK-Y342A and the constitutively active BRK-YF. We observed that BRK-W44A, ΔSH2-BRK, BRK-WT, BRK-Y342A, and BRK-YF all coprecipitated with GFP-SMAD4. In contrast, ΔSH3-BRK did not coprecipitate with GFP-SMAD4, suggesting that the SH3 domain is necessary for BRK/SMAD4 interaction (Fig. 2D). In a similar fashion, we mapped domains of SMAD4 essential for interaction with BRK. We expressed BRK-YF in HEK293T cells together with full-length Halo-SMAD4 or with several SMAD4 truncation mutants (described in Fig. 2E) and captured protein complexes by Halo affinity purification. We found SMAD4 mutants that contained either the MH1 domain or the MH2 domain (mutants A, B, D, and E) interacted with BRK-YF. The MH1 domain showed a higher affinity for BRK-YF than the MH2 domain (compare Fig. 2E, lanes B and D), while the linker region alone showed a very weak affinity for BRK-YF (Fig. 2E, lane C). Protein interactions were further analyzed by affinity purification followed by mass spectrometry (APMS) of Halo-SMAD4 ectopically expressed by itself or coexpressed with either SF-BRK-WT or SF-BRK-YF in HEK293T cells. Halo affinity purification followed by MudPIT proteomics analyses showed that Halo-SMAD4 associated proteins (fig. S2, A to C, and table S1) and the expression of Halo-SMAD4 in those cells (fig. S2D) and was able to pull down both BRK-WT and BRK-YF (Fig. 2F and table S1). The interaction was shown to be reciprocal when SNAP-Flag-BRK-YF copurified with Halo-SMAD4 in the SNAP affinity purification analyzed by MudPIT (fig. S2E). These APMS experiments hence confirmed the conclusion from the coimmunoprecipitation experiments: BRK interacts with SMAD4.

Next, we examined whether Halo-SMAD4 and SF-BRK-YF colocalize in vivo. We used live-cell imaging to assess the localization of ectopically expressed Halo-SMAD4 and SF-BRK-YF in HEK293T cells. Halo-SMAD4 and SF-BRK-YF were transfected in HEK293T cells either alone or together and were imaged by confocal microscopy (Fig. 2G). We observed that Halo-SMAD4 predominantly localized to the cytosol (Fig. 2G, top), while SNAP-Flag-BRK-YF localized both in the cytosol and nucleus (Fig. 2G, middle). However, Halo-SMAD4 and SNAP-FLAG-BRK-YF did colocalize in the cytosol (Fig. 2G, bottom) when cotransfected in HEK293T cells. In addition, immunocytochemistry experiments revealed that the endogenous BRK and SMAD4 colocalized in MCF7 cells (fig. S2F). Together, our observations support that SMAD4 is a cytosolic BRK interaction partner in cells, which is consistent with a potential role of SMAD4 as a target of BRK phosphorylation.

Activated BRK phosphorylates SMAD4 on residues Tyr^{353} and Tyr^{412}

We have shown that activated BRK interacts with SMAD4 and colocalizes with SMAD4 in the cytosol of live cells. Given that BRK is a nonreceptor tyrosine kinase, we asked whether activated BRK phosphorylates SMAD4. To selectively identify BRK-mediated SMAD4 phosphorylation, we expressed Halo-SMAD4 alone or in combination with SF-BRK-YF in HEK293T cells and affinity-purified SMAD4 to analyze posttranslational modifications by mass spectrometry (Fig. 3A). Although prior studies had reported several serine, threonine, and tyrosine phosphorylation sites within SMAD4 (Fig. 3B; source: PhosphoSitePlus), our MudPIT-APMS approach identified several previously unknown phosphorylation sites on SMAD4 in the presence or absence of SNAP-Flag-BRK-YF (table S2). We found that Halo-SMAD4 displayed three unique phosphorylations on serine(S)-344, tyrosine(Y)-353, and tyrosine(Y)-412 in the presence of activated BRK (Fig. 3B). Unexpectedly, one of these phosphorylation sites was S-344, which raises the intriguing possibility that activated BRK may be a dual-specificity kinase, such as MAPK kinase kinases, which are involved in MAP pathways (*18*). However, since BRK is known to potentiate several signaling pathways, including the MAPK signaling pathway, it is possible that the S-344 phosphorylation is an indirect effect. Nonetheless, since BRK is a tyrosine kinase, we focused to further validate the phosphorylation of Y353 and Y412 (Fig. 3B). We implemented a multiple-reaction monitoring (MRM) approach to specifically targeting the peptides bearing these phosphorylated and nonphosphorylated tyrosines (Fig. 3C and fig. S3, A and B). For both

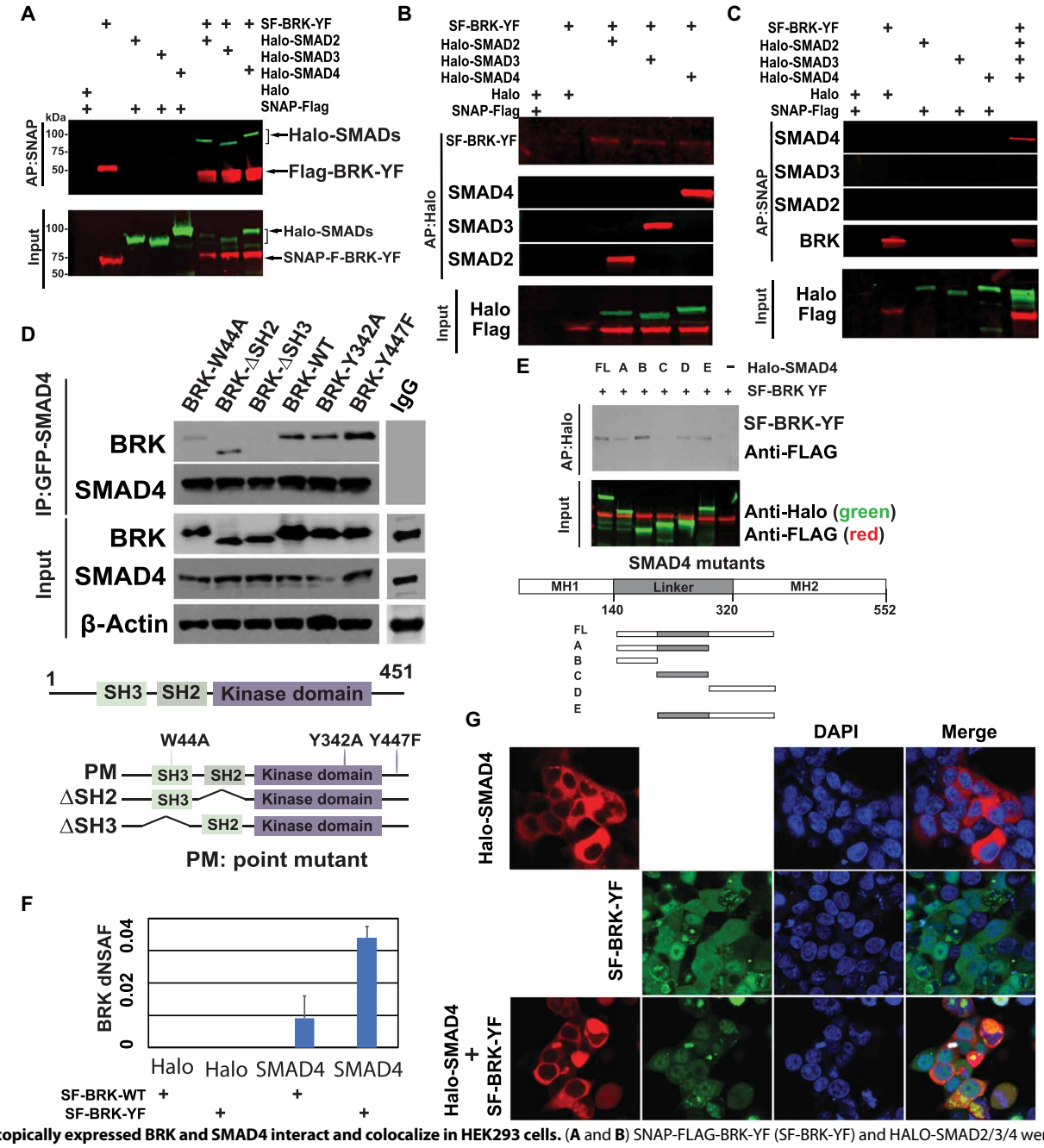

Fig. 2. Ectopically expressed BRK and SMAD4 interact and colocalize in HEK293 cells. (**A** and **B**) SNAP-FLAG-BRK-YF (SF-BRK-YF) and HALO-SMAD2/3/4 were expressed into HEK293 cells, and cell lysates were subjected to affinity purification (AP) with Halo magnetic beads (A) or SNAP capture magnetic beads (B) antibodies, followed by immunoblotting using anti-Halo and anti-FLAG antibodies. Bottom: The ectopic expression of BRK and SMAD2/SMAD3/SMAD4 as detected by anti-Halo and anti-FLAG antibodies. During affinity purification, either the SNAP_Flag or Halo tags were clipped off using Precision or Tev proteases, respectively. Halo-SMAD4 is ~93 kDa; after Halo-Tag removal, SMAD4 is ~60 kDa. Similarly, SNAP-Flag-BRK is ~73 kDa, and after SNAP-Tag removal, BRK is ~50 kDa. In (B), the three different blots in the middle were probed with the SMAD2, SMAD3, and SMAD4 antibodies. (**C**) HEK293 cells were cotransfected with SF-BRK-YF, Halo-SMAD2, Halo-SMAD3, and Halo-SMAD4, and the cell lysates were subjected to affinity purification with Halo magnetic beads or SNAP capture magnetic beads, followed by immunoblotting using anti-SMAD2, anti-SMAD3, anti-SMAD4, and anti-Flag antibodies. Total cell lysates were also analyzed by immunoblotting using antibodies against Halo-SMAD2, Halo-SMAD3, Halo-SMAD4, and Flag. (**D**) GFP-SMAD4 was cotransfected with BRK-W44A, BRK-ΔSH2, BRK-ΔSH3, BRK-WT, BRK-Y342F, or BRK-YF. The corresponding protein extracts were immunoprecipitated with anti-GFP and mouse immunoglobulin G (IgG; lysates from SMAD4 and BRK-YF cotransfected cells as a representative) and immunoblotted with anti-BRK and anti-GFP antibodies and β-actin as a loading control. IP, immunoprecipitation. (**E**) SF-BRK-YF was expressed either alone or with Halo-SMAD4 [full length (FL)] or SMAD4 deletion mutants (A to E) in HEK293 cells. Total cell lysates were subjected to Halo affinity purification and analyzed by immunoblotting with FLAG and Halo antibodies. (**F**) Halo-SMAD4 or Halo plasmid alone with SF-BRK-WT or SF-BRK-YF was ectopically expressed in HEK293T cells. SNAP affinity purification followed by MudPIT mass spectrometry analysis showed that Halo-SMAD4 copurified with SNAP-Flag-BRK-WT or SNAP-Flag-BRK-YF but not with Halo alone. (**G**) Halo-SMAD4 or SF-BRK-YF alone or in combination was transfected into HEK293T cells. Halo-Tag TMRDirect fluorescent ligand (red) and SNAP-Cell 505-Star (green) were used to label Halo-Tag and SNAP-Tag proteins, respectively; DNA was stained with Hoechst dye (blue). DAPI, 4′,6-diamidino-2-phenylindole.

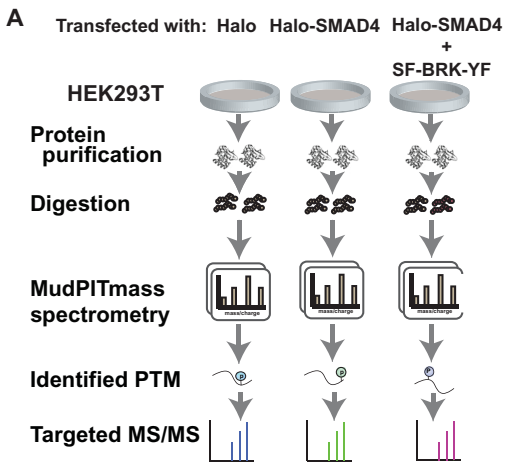

B

Phosphorylated SMAD4 residue	Previously reported[a]	Halo-SMAD4 Detected of 3 Replicates	Halo-SMAD4 Modified_SpC	Halo-SMAD4+BRK-YF Detected of 2 Replicates	Halo-SMAD4+BRK-YF Modified_SpC
S138	x	3	63	2	35
S403		1	14	2	13
S357		2	4	0	0
S517		2	3	0	0
Y513	x	2	3	0	0
S343	x	0	0	1	2
S344		0	0	1	2
Y353		**0**	**0**	**2**	**3**
Y412		**0**	**0**	**1**	**1**

[a] www.phosphosite.org

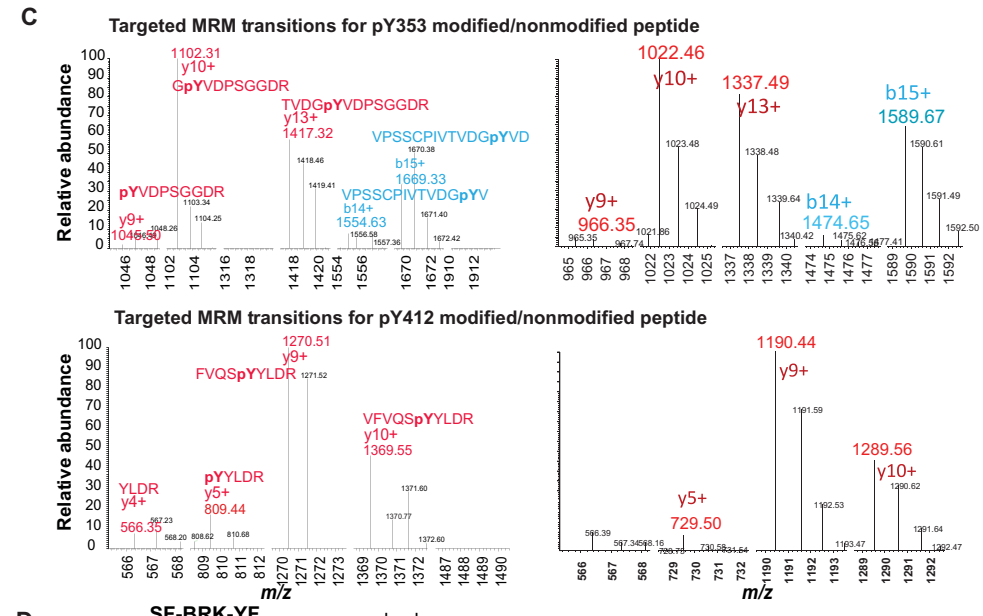

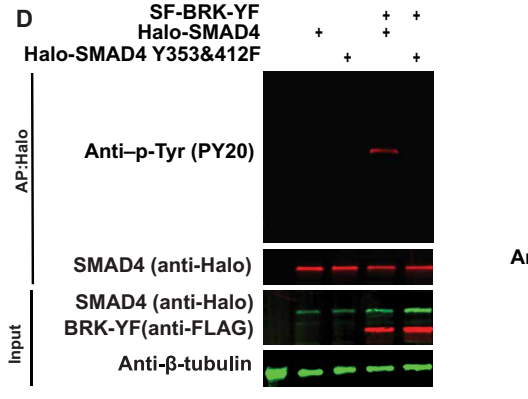

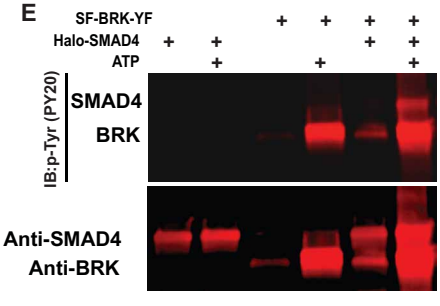

Fig. 3. Targeted proteomics reveals BRK-mediated tyrosine phosphorylation of SMAD4. (**A**) Workflow of global phosphorylation analysis by MudPIT mass spectrometry and targeted proteomics. MS/MS, tandem mass spectrometry. (**B**) Phosphorylation sites identified in this study (S, serine; T, threonine; Y, tyrosine) tabulated with known phosphorylation sites (www.phosphosite.org/proteinAction.action?id=1845&showAllSites=true on 7 February 2018). The frequency of detection and total spectral counts for the phosphorylated peptides are reported for the Halo-SMAD4 affinity purifications with or without BRK-YF. (**C**) Validation of previously unidentified tyrosine phosphorylations on Halo-SMAD4 Y353 and Y412 in the presence of SF-BRK-YF by MRM. For each phosphopeptide, at least four fragment ions containing the modified residue were targeted for MRM including respective nonmodified resides. (**D**) Halo-SMAD4 or Halo-SMAD4 Y353F and Y412F, with or without SNAP-Flag-BRK-YF were cotransfected into HEK293T cells, and the cell lysates were subjected to affinity purification, followed by immunoblotting (IB) with anti-PY20 or anti-SMAD4 antibodies. The expression of Halo-SMAD4, Halo-SMAD4 Y353F and Y412F, and SNAP-Flag-BRK-YF were analyzed by immunoblotting using anti-Halo and anti-Flag specific antibodies. β-Tubulin was used as a loading control. (**E**) An in vitro kinase assay was performed using the active kinase, Flag-BRK, and the substrate SMAD4, in the presence or absence of adenosine 5′-triphosphate (ATP). Antiphosphotyrosine antibody PY20 was used to detect phosphotyrosine. The blots were reprobed with anti-Flag and anti-SMAD4 antibody (bottom).

phosphorylated and nonphosphorylated sites, the transitions of at least four fragment ions bearing the modified/nonmodified residues were targeted for MRM (Fig. 3C, left modified and right nonmodified) and were detected in the protein sample from the affinity-purified Halo-SMAD4 or Halo-SMAD4 cotransfected with BRK-YF (Fig. 3C). In addition, the tandem mass spectrometry spectra that were acquired immediately after the MRM spectra mapped to the expected phosphorylated peptides (fig. S3, A and B).

To further validate BRK-mediated phosphorylation of SMAD4 Y353 and Y412, we next generated a mutant of SMAD4 lacking these two tyrosine residues (Halo-SMAD4 Y353F and Y412F). We first affinity-purified Halo-SMAD4 from cells coexpressing BRK-YF with Halo-SMAD4 and analyzed the pulled-down proteins with an antibody specific to phosphorylated tyrosines, PY20 (Fig. 3D). We detected phosphorylated SMAD4 in the presence of BRK-YF but not in the absence of BRK-YF (Fig. 3D, lane 4). However, in the mutant Halo-SMAD4 Y353F and Y412F, we could not detect a similar band indicating the phosphorylation (Fig. 3D, lane 5). In light of these findings, we tested whether SMAD4 is a direct substrate of BRK. In an in vitro kinase assay, which was accomplished using BRK-YF and the SMAD4, we observed phosphorylation of SMAD4 in the presence of BRK-YF, confirming that SMAD is a direct substrate of BRK (Fig. 3E, lane 6, top). We also observed the kinase activity of autophosphorylated BRK-YF (Fig. 3E, lanes 3 and 5, top). Our biochemical and mass spectrometry analysis of phosphorylated peptides from SMAD4 indicates that two previously unidentified tyrosine residues were phosphorylated explicitly by BRK. These sites were confirmed as phosphorylated with an orthogonal MRM mass spectrometry approach and by site-directed mutagenesis combined with Western blotting. These two tyrosines are located within SMAD4 MH2 domain, which is the most frequently mutated in cancers, and are likely involved in regulating the SMAD4 protein interaction network.

BRK and SMAD4 protein expression levels are inversely correlated in most breast cancer cells and tissues

Since SMAD4 is a tumor suppressor (*14*, *12*) and we and others have previously shown that BRK acts as an oncogene (*2*, *10*, *6*), we opted to explore the possible connection between SMAD4 and BRK protein levels in breast cancer cells and tissues. First, we examined the endogenous protein expression of SMAD4 and BRK to determine the expression profiles of these proteins in breast cancer cells. Using antibodies against each protein, we evaluated the expression level of SMAD4 and BRK in a panel of 10 breast cancer cells, two immortalized cell lines commonly used to model nondiseased human mammary epithelial cells (MCF10A and MCF12F), and lastly in HEK293 cells. We detected SMAD4 in MCF10A, MCF12F, and HEK293 and in six breast cancer cell lines MDA231, Hs578T, T47D, BT549, MCF7, and BT474. SMAD4 expression was very low or undetectable in four other breast cancer cell lines: BT20, HCC1428, SKBR3, and HCC1954 (Fig. 4A). Detectable amounts of BRK were observed in BT20, HCC1428, SKBR3, T47D, MCF7, BT474, and HCC1954, but not in MDA231, Hs578T, BT549, and HEK293 cells, while very low expression was observed in MCF10A and MCF12F (Fig. 4A). The levels of SMAD4 and BRK were inversely correlated in MCF10A, MCF12F, MDA-MB-231, BT20, HCC1428, SKBR3, Hs578T, BT549, HCC1954, and HEK293. In particular, the expression of SMAD4 and BRK in all of the triple-negative breast cancer (TNBC) cells we tested (MDA231, BT20, Hs578T, BT549, and HCC1954) showed this inverse expression pattern (Fig. 4A).

These diverse patterns of BRK/SMAD4 protein levels might be explained by differences in BRK or SMAD4 mRNA levels. To compare the gene expression pattern of *SMAD4* and *BRK*, we examined RNA sequencing data from the Cancer Cell Line Encyclopedia (https://portals.broadinstitute.org/ccle) corresponding to the 10 breast cancer cell lines that we had analyzed. Unexpectedly, we observed that *SMAD4* and *BRK* showed similar patterns of mRNA expression in all 10 breast cancer lines including TNBC cells (Fig. 4B and fig. S4A), suggesting that the effects we had initially noticed were likely regulated at the protein level rather than mRNA expression. Next, to reinforce the evidence obtained using cancer cell lines, we mined data from patient tumor samples (*19*) to determine SMAD4 and BRK protein expression patterns in three major breast cancer subtypes: estrogen/progesterone (ER/PR) positive, HER2 positive, and TNBC. Again, we observed that SMAD4 and BRK were inversely expressed in these breast cancer subtypes (Fig. 4C).

To further interrogate the relationship between SMAD4 and BRK expression, we stably expressed constitutively active BRK (BRK-YF) into three cell lines that expressed SMAD4 but not BRK (HEK293, MDA-MB-231, and MCF10A cell lines). An elevated level of phosphorylation of cellular targets was observed in the cells stably expressing GFP-BRK-YF, as visualized by immunoblotting with an antiphosphotyrosine antibody (4G10) (Fig. 4D). We therefore examined the expression of SMAD4 in BRK-YF–expressing cells and observed a sharp reduction of endogenous SMAD4 protein in all three of the cell lines expressing activated BRK compared to those parental cells (Fig. 4D). However, we did not observe any noticeable change in the endogenous protein levels of SMAD2 and SMAD3 (Fig. 4D), suggesting that the effect that activated BRK had on protein levels was specific to SMAD4. Next, we examined the expression of SMAD4 transcripts in SF-BRK-YF–transduced HEK293 cells by quantitative reverse transcription polymerase chain reaction (qRT-PCR) using SMAD4-specific primers. The qRT-PCR analysis showed no significant difference between the SMAD4 mRNA levels in SF-BRK-YF–expressing cells compared with the control cells (fig. S4B). In addition, to interrogate whether SF-BRK-YF regulates SMAD4 via the ubiquitin-proteasome pathway, we tested SMAD4 protein levels in SF-BRK-YF–expressing cells in the presence or absence of the peptide-aldehyde proteasome inhibitor MG132 (carbobenzoxyl-L-leucyl-L-leucyl-L-leucine). We found that MG132 treatment rescued the SMAD4 protein levels in SF-BRK-YF–expressing HEK293 cells (Fig. 4E).

Last, since our data showed that SMAD4 and BRK protein levels were inversely correlated, we asked whether knocking down BRK by short hairpin RNA (shRNA) could modulate the levels of SMAD4 in MCF7 cells. MCF7 cells were selected because both SMAD4 and BRK proteins were moderately expressed in these cells (Fig. 4A). We attained a 70 to 80% reduction of BRK in MCF7 cells (fig. S4C). However, we did not observe any noticeable effect on the expression of SMAD4 protein in MCF7 cells with depleted BRK (fig. S4C). Since the depletion of BRK did not affect the expression of SMAD4, we aimed to assess the expression of a known target of SMAD4 in GFP-BRK-YF cells. As a proof of principle, we evaluated the expression of p21, a known target of SMAD4 (*20*), in the cells stably expressing GFP-BRK-YF and the parental cell lines. We found that p21 protein levels and mRNA level sharply decreased in the cells expressing activated BRK compared to parental cells (Fig. 4F and fig. S4D). Moreover, reduction of p21 induced by constitutively active BRK-YF could be rescued by ectopically overexpressed GFP-SMAD4

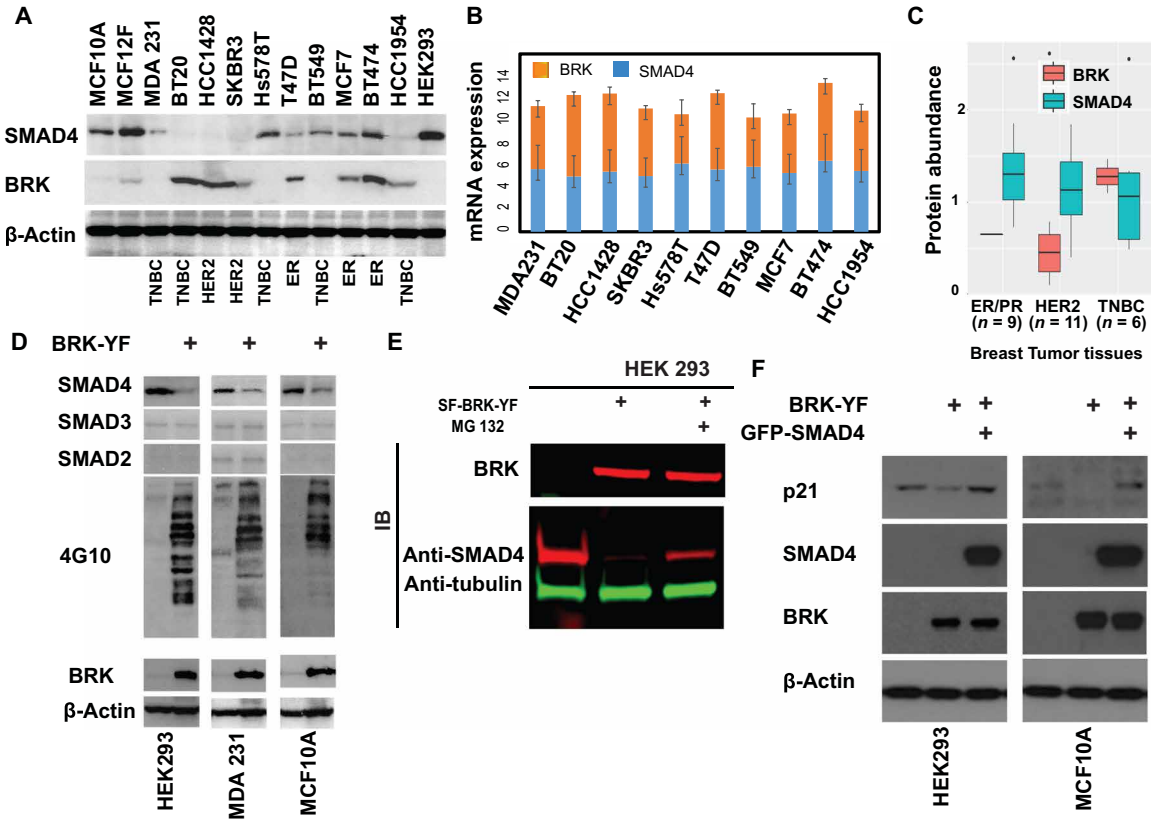

Fig. 4. BRK and SMAD4 are expressed in most breast cancer cells and tissues. (**A**) BRK expression was detected by immunoblotting in the indicated normal mammary epithelial and breast cancer cell lines (TNBC, HER2, and ER), and β-actin was used as a loading control. (**B**) Differential expression of *SMAD4* and *BRK* in breast cancer cell lines, as obtained from the Cancer Cell Line Encyclopedia. (**C**) Absolute expression of BRK and SMAD4 in patient-driven tumor tissues of three major breast cancer subtypes: ER/PR, HER2, and TNBC. Super-stable isotope labeling by amino acids–based absolute proteins expression data were obtained from Tyanova *et al*. (*19*). (**D**) Immunoblotting analysis of total cell lysates from HEK293, MDA231, and MCF10A cells with or without ectopically expressed GFP-BRK-YF. Stable cell lysates were analyzed by immunoblotting using SMAD2, SMAD3, SMAD4, antiphosphotyrosine (4G10), and GFP antibodies. β-Actin served as a loading control. (**E**) SF-BRK-YF was ectopically expressed in HEK293 cells and treated with MG132 for 8 hours, followed by immunoblotting analysis using Flag and SMAD4 antibodies. β-Tubulin served as a loading control. (**F**) Total cell lysates from HEK293 and MCF10A; GFP-BRK-YF–expressing HEK293 and MCF10A stable cell lines and GFP-SMAD4–transfected GFP-BRK-YF–expressing stable HEK-293 and MCF10A stable cell lines were analyzed by immunoblotting using p21, SMAD4, and BRK-specific antibodies. β-Actin was a loading control.

(Fig. 4F and fig. S4C), suggesting that large amounts of the GFP-SMAD4 compensated for the degradation of endogenous SMAD4 mediated by BRK-YF phosphorylation, hence restoring the downstream expression of the p21 protein.

Overall, our data indicate that, compared with control cells, the increased levels of BRK observed in several breast cancer cell types were concomitant with reduced levels of SMAD4 and that changes in protein level did not necessarily result from changes in BRK/SMAD4 mRNA levels. In addition, introducing the active BRK-YF into cells expressing SMAD4 resulted in reduced levels of SMAD4. As BRK and SMAD4 showed similar mRNA expression patterns but differ in protein levels and the reduced SMAD4 protein can be rescued by MG132 treatment, it is possible that BRK suppresses SMAD4 through the ubiquitin/proteasome pathway.

SMAD4 is a target of ubiquitin modification enzymes in the presence of activated BRK

Since we had found that BRK phosphorylates SMAD4 (Fig. 3) and SMAD4 levels were markedly lower in stably expressing BRK-YF cells (Fig. 4D), we next examined whether the presence of BRK-WT/BRK-YF made Halo-SMAD4 a potential target of the ubiquitin-proteasome machinery. To interrogate the impact of constitutively active BRK on SMAD4 ubiquitination, we used our established workflow (*21*) for Halo/MudPIT APMS analysis (Fig. 5A and fig. S5A). We first expressed Halo-SMAD4 in the presence or absence of SF-BRK-WT or SF-BRK-YF and purified Halo-SMAD4–associated proteins by affinity chromatography. We identified SMAD4-associated proteins by MudPIT mass spectrometry (fig. S2, A to C). We found that Halo-SMAD4 recruited several ubiquitin and deubiquitin ligases in the presence of BRK-WT/BRK-YF (fig. S5D and table S1). SMAD4 interacted with the deubiquitin ligases ubiquitin specific peptidase 9 X-linked (USP9X), ubiquitin specific peptidase 32 (USP32), and ubiquitin specific peptidase 7 (USP7) in the presence of both BRK-WT and BRK-YF. However, SMAD4 association with the ubiquitin ligases HECT and RLD domain containing E3 ubiquitin protein ligase 2 (HERC2) and ring finger protein 138 (RNF138) were up-regulated only in the presence of BRK-YF. Since Halo-SMAD4 interacted with ubiquitin ligases in the presence of activated BRK, we then tested the possibility that the BRK-mediated phosphorylation of SMAD4 facilitated its degradation through the ubiquitin/proteasome system (*22*). Halo-SMAD4, BRK-YF, and hemagglutinin (HA)–ubiquitin were expressed in HEK293T cells in the combinations shown in Fig. 5B,

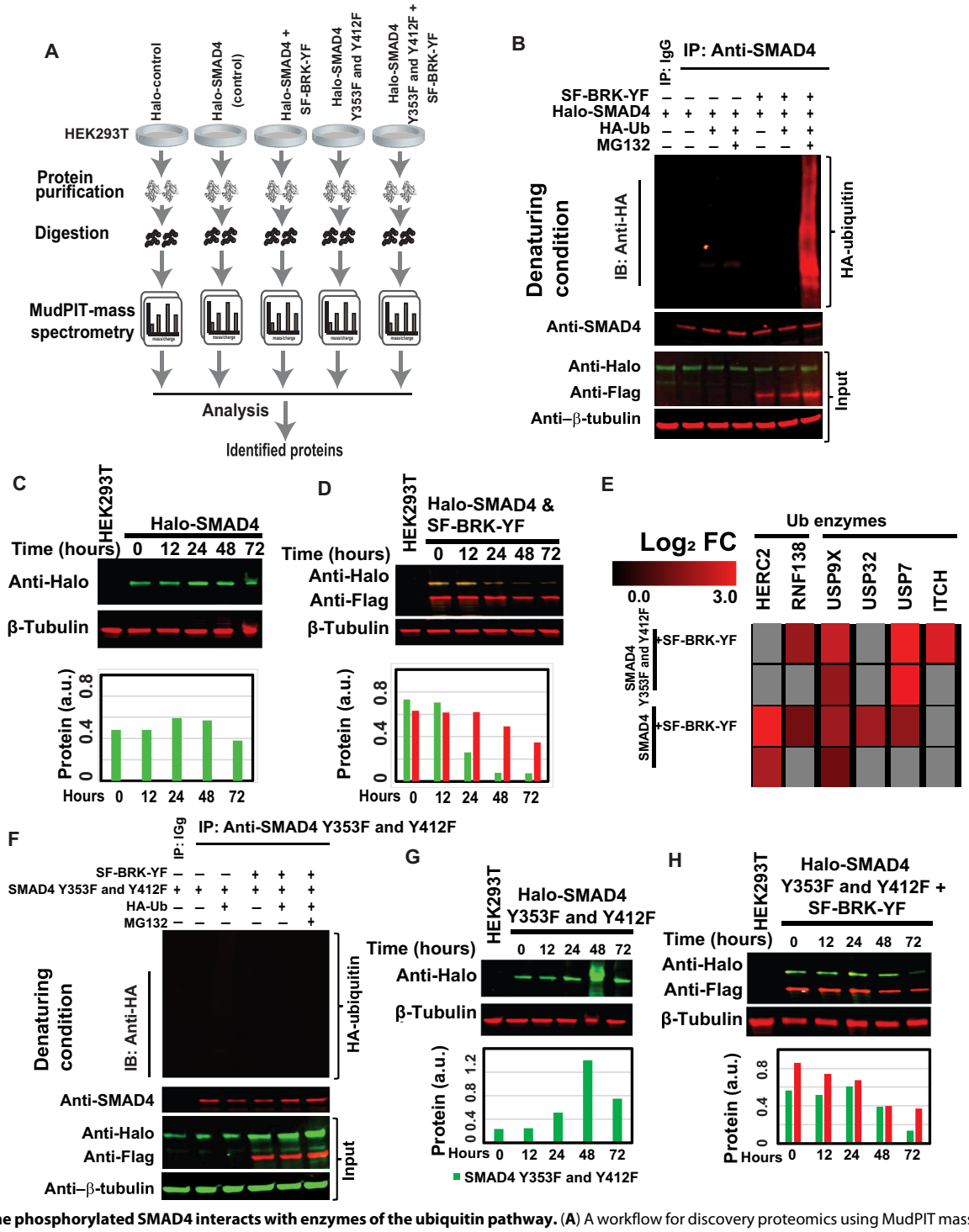

Fig. 5. Tyrosine phosphorylated SMAD4 interacts with enzymes of the ubiquitin pathway. (**A**) A workflow for discovery proteomics using MudPIT mass spectrometry for protein identifications. (**B**) SMAD4 polyubiquitination under denaturing condition: HEK293T cells were transiently transfected with Halo-SMAD4, SF-BRK-YF, or in combination with HA-ubiquitin plasmid. After 36 hours, the cells were treated with 10 μM MG132 for an additional 8 hours. The total cell lysates were subjected to immunoprecipitation, followed by immunoblotting with anti-HA and anti-SMAD4 antibodies. (**C** and **D**) SMAD4 stability: Tet-On–inducible Halo-SMAD4 plasmid alone or Tet-On–inducible Halo-SMAD4 plasmid with SNAP-Flag-BRK-YF was transfected into HEK293T cells for the indicated time points and analyzed by immunoblotting with anti-Halo, anti-Flag, and β-tubulin antibodies. The protein expression was quantified using ImageJ software and plotted as a bar chart. (**E**) Interaction with ubiquitin modifying enzymes: Relative QSPEC $\log_2$ fold changes measured for the specified proteins in the APMS analyses of Halo-SMAD4/Halo-SMAD4 Y353F and Y412F with or without BRK-YF were plotted as heat maps (Genesis software package developed by A. Sturn and R. Snajder: http://genome.tugraz.at/genesisclient/genesisclient_description.shtml). (**F**) SMAD4 Y353F and Y412F polyubiquitination under denaturing condition: HEK293T cells were transiently transfected with Halo-SMAD4 Y353F and Y412F or SF-BRK-YF or in combination with HA-ubiquitin plasmid and analyzed as described above. (**G** and **H**) SMAD4 stability: Tet-On–inducible Halo-SMAD4 Y353F and Y412F plasmid with or without SNAP-Flag-BRK-YF was transfected into HEK293T cells and analyzed as described above. a.u., arbitrary units.

and cells were treated with or without MG132. We examined SMAD4 protein for ubiquitination both under normal and denaturing conditions by resolving SMAD4 immunoprecipitated samples by SDS–polyacrylamide gel electrophoresis (PAGE) and immunoblotting using anti-HA antibody. Our data showed a smear of ubiquitin-conjugated SMAD4 in the presence of proteasome inhibitor (Fig. 5B and fig. S5E, lane 5), which was not apparent in controls (Fig. 5B and fig. S5E, lanes 1 to 4). Our results led us to conclude that the presence of activated BRK causes the down-regulation of SMAD4 by the ubiquitin/proteasome degradation pathway.

To investigate the rate of proteasomal degradation of SMAD4 in the presence or absence of BRK-YF, we expressed Halo-SMAD4 in HEK293T cells under the control of a tetracycline-inducible promoter, with or without BRK-YF. Twenty-four hours after transfection, tetracycline-containing medium was replaced with regular HEK293T cell culture media, and cells were periodically harvested as indicated in Fig. 5 (C and D). Immunoblotting of cell lysates showed that Halo-SMAD4 protein levels were markedly reduced in the presence of activated BRK as early as 24 hours (Fig. 5D), while in the absence of BRK-YF, Halo-SMAD4 protein levels had not significantly decreased even after 72 hours (Fig. 5C). This difference in protein stability is hence consistent with a role for BRK in regulating SMAD4 degradation. In summary, our data indicate that ubiquitin ligases are recruited to phosphorylated SMAD4 in the presence of BRK-YF, leading to its degradation by the proteasome.

BRK-mediated phosphorylation of tyrosine-353 and tyrosine-412 of SMAD4 is required for ubiquitination and degradation of SMAD4

To gain further mechanistic insight, we again used Halo-MudPIT APMS to explore the BRK-YF–modulated SMAD4 ubiquitination and degradation using a mutant of SMAD4 (Halo-SMAD4 Y353F and Y412F) that could not be phosphorylated on tyrosine residues Y353 and Y412 (Fig. 5A). As we have described previously with Halo-SMAD4, we analyzed the Halo-SMAD4 Y353F&Y412F–associated proteins with or without BRK-YF and established that baits were present in all affinity purifications (fig. S5, B and C, and table S1). We found that in the presence of the BRK-YF, RNF138 (a ubiquitin ligase) interacted with Halo-SMAD4 but not with SMAD4 Y353F and Y412F, suggesting that the presence of the BRK-YF is necessary for this interaction. Similarly, SMAD4 interaction with the ubiquitin ligase HERC2 was significantly augmented in the presence of activated BRK, and this interaction was completely lost with mutant Halo-SMAD4 Y353F and Y412F (Fig. 5E and table S1). Curiously, itchy E3 ubiquitin protein ligase (ITCH) showed a stronger affinity for Halo-SMAD4 Y353F and Y412F in comparison to Halo-SMAD4 in the presence of activated BRK and did not interact in the absence of BRK. Considering the deubiquitinases, we noticed that USP9X and USP7 showed a higher affinity for Halo-SMAD4 Y353F and Y412F in the presence of activated BRK and that the deubiquitinase USP32 interacted only with Halo-SMAD4 in the presence of activated BRK (Fig. 5E). Similar to BRK, USP32 is also often overexpressed in breast cancer cells and tumors, and its inhibition reduces cell proliferation, migration, and apoptosis (*23*).

Since our proteomics data (Fig. 5E) showed that phosphorylation of Y353 and Y412 of SMAD4 is essential for ubiquitin ligase recognition, we tested whether the mutant SMAD4 escaped BRK-regulated proteasomal degradation. Plasmids expressing Halo-SMAD4 Y353F and Y412F, SNAP-Flag-BRK-YF, and HA-ubiquitin were transfected into HEK293T cells. The transfected cells were treated with MG132 for 8 hours to inhibit 26*S* proteasome. After Halo affinity purification, we analyzed purified samples for ubiquitinated proteins using an anti-HA antibody. Our data showed that ubiquitin was unable to conjugate with mutant Halo-SMAD4 Y353F and Y412F to mark it for proteasomal degradation (Fig. 5F and fig. S5F). Our findings strongly suggest that tyrosine-353 and tyrosine-412 of SMAD4 are essential for SMAD4 ubiquitination.

Since the Halo-SMAD4 Y353F and Y412F was not ubiquitinated, we next examined the stability of SMAD4 Y353F and Y412F in the presence or absence of BRK-YF. To this end, we transfected tetracycline-inducible Halo-SMAD4 Y353F and Y412F alone or with BRK-YF into HEK293T cells. We found that Halo-SMAD4 Y353F and Y412F protein levels remained stable for a longer time in the absence of activated BRK (Fig. 5, G and H). We also found that the mutant SMAD4 was more stable in the presence of BRK-YF than the WT SMAD4 protein (compare to Fig. 5D). These findings are consistent with a model whereby BRK-mediated phosphorylation of SMAD4 accelerates its proteasomal degradation, while the phosphorylation-incompetent mutant SMAD4 Y353F and Y412F escapes ubiquitination and subsequent degradation.

BRK represses the FRK tumor suppressor in a SMAD4-dependent manner to induce EMT and cell invasion

Since SMAD4 is a transcription factor and phosphorylated SMAD4 interacts with chromatin remodeling complexes (fig. S6, A and B, and table S3), we next investigated genes that might be targeted by SMAD4. We performed an in silico analysis to identify potential SMAD4 binding sites in the genome. We found putative SMAD4-binding sites in the promoter of several genes, including tumor suppressor *FRK* (*24*). Chromatin immunoprecipitation (ChIP)–sequencing data (Gene Expression Omnibus: GSE96401; www.encodeproject.org/experiments/ENCSR826YMT/) also showed that SMAD4 binds the transcription start sites of *FRK* in HepG2 cells (fig. S7A). This finding spurred our interest to further investigate a potential connection between BRK-mediated SMAD4 regulations of FRK expression. To test our hypothesis that SMAD4 regulates this promoter, we performed a luciferase reporter assay and found that luciferase activity was twofold higher in lysates from cells coexpressing SMAD4 and the *FRK* promoter, suggesting that SMAD4 positively regulates the promoter activity of *FRK* (Fig. 6A), consistent with the presence of SMAD4 binding sites in the *FRK* promoter. In addition, we performed ChIP-qPCR experiment and found SMAD4 binds to the transcription start sites of *FRK* in MCF7 cells (Fig. 6B). Next, we compared the mRNA expression of *FRK* in MDA-MB-231 cells (which express SMAD4, but not BRK—see Fig. 4A) with *FRK* expression in MDA-MB-231 cells stably expressing BRK-YF. Consistent with BRK-YF–mediated degradation of SMAD4, *FRK* mRNA levels were very low in the cells stably expressing BRK-YF. However, overexpressing SMAD4 in the MDA231-BRK-YF cells restored the expression of *FRK* mRNA (Fig. 6C). In addition, we observed that stably expressing BRK-YF decreased the FRK protein levels in MDA231 cells (Fig. 6D, compare lanes 1 and 2) and that FRK protein levels were restored by overexpressing SMAD4 (Fig. 6D).

It has been reported that FRK suppresses EMT and inhibits cancer metastasis (*25*), while TGF-β/SMAD4 signaling is crucial for EMT and promotes metastasis (*26*). We deduced that the SMAD4-dependent control of *FRK* expression might consequently be controlling the expression of EMT markers. To this end, we examined the expression

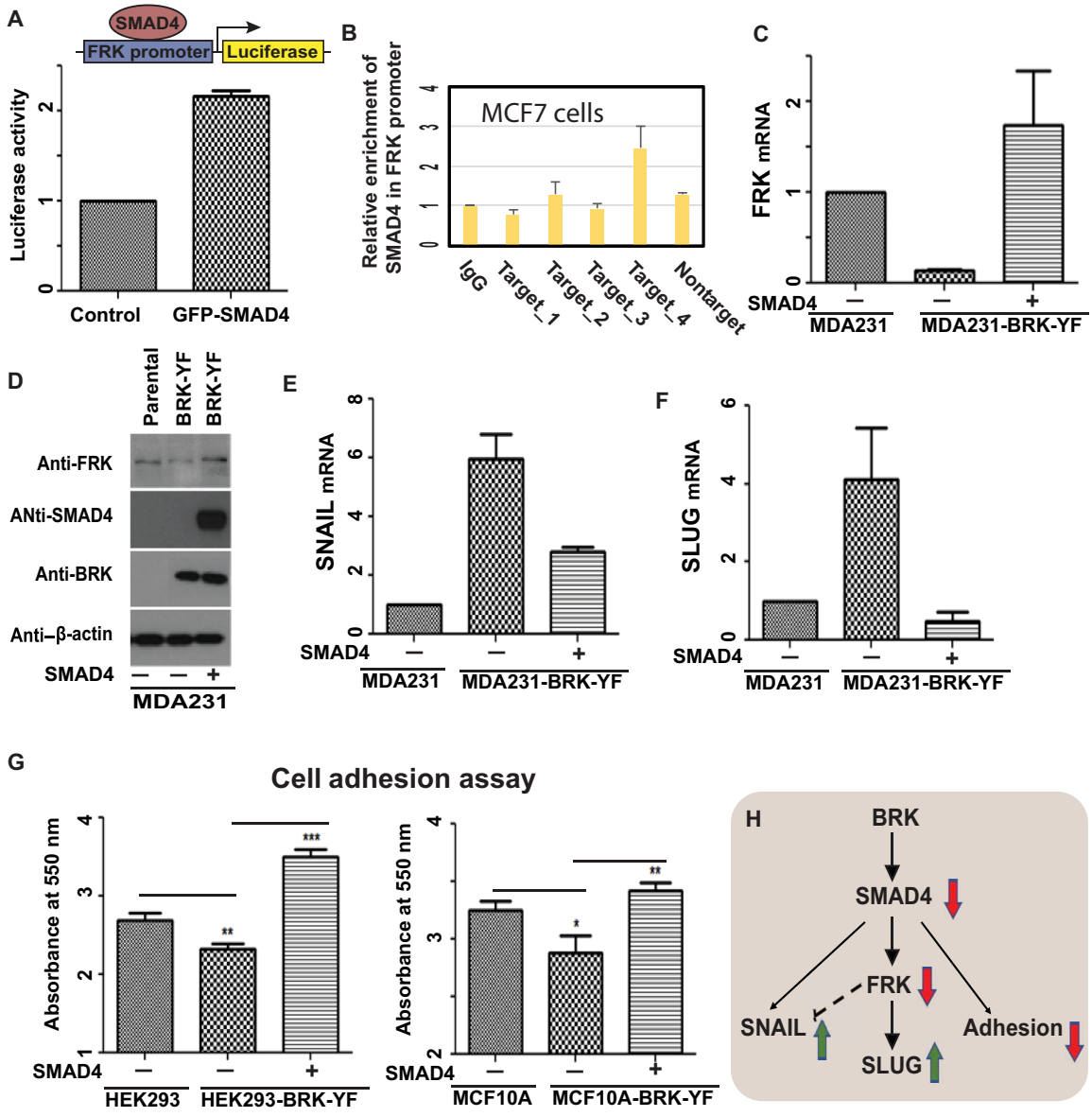

Fig. 6. BRK regulates tumor suppressor, EMT markers, and metastatic potential in a SMAD4-dependent manner. (**A**) Luciferase reporter constructs were transfected in HEK293 cells with and without SMAD4 to measure the transcriptional activation of the *FRK* promoter. (**B**) ChIP-qPCR experiment shows the relative abundance of SMAD4 in FRK promoter. (**C** and **D**) The mRNA levels of *FRK* were quantified via quantitative RT-PCR and protein levels were analyzed by immunoblotting of the total proteins extracted from parental, stably expressing BRK-YF and SMAD4-transfected BRK-YF expressing MDA-MB-231 stable cell lines. (**E** and **F**) The mRNA levels of *SNAIL* and *SLUG* were quantified via quantitative RT-PCR in the parental cell line, BRK-YF stable expressing MDA-MB-231 cell line and ectopically expressed SMAD4 in BRK-YF expressing stable cell line. (**G**) Cell adhesion assay shows the cell adhesion properties of HEK293 and MCF10A, BRK-YF stably expressing HEK293 and MCF10A cell lines and SMAD4-transfected stable cell lines. $^{*}P \leq 0.05$; $^{**}P \leq 0.001$; $^{***}P \leq 0.0001$. (**H**) Activated BRK regulates EMT markers (SNAIL and SLUG) and cell adhesion by modulating SMAD4-FRK.

of EMT markers (E-cadherin, N-cadherin Twist, vimentin, fibronectin, SLUG, and SNAIL) in parental and BRK-YF–expressing MDA-MB-231 cells. We found that *SLUG* and *SNAIL* expression increased in MDA-MB-231 cells stably expressing BRK-YF in comparison to parental cells (six- and fourfolds higher, respectively; Fig. 6, E and F). In addition, SLUG but not SNAIL was significantly suppressed in stably FRK-YF–expressing MDA-MB-231 cells (fig. S7B, C and D). Moreover, ectopically expressed SMAD4 suppressed the BRK-YF–mediated induction of *SNAIL* and *SLUG* (Fig. 6, E and F). We did not observe any change in the other EMT markers tested (data not shown). Last, since our proteomics data showed that the presence of BRK-YF reduced the interaction of SMAD4 with cell adhesion molecules (table S1), we examined the cell adhesion properties of the BRK-YF–expressing HEK293 and MCF10A cells. We found that activated BRK reduced the cell adhesion capability of BRK-YF–expressing cells and that adhesion capability could be completely restored by overexpressing SMAD4 (Fig. 6G). Overall, our data suggest that activated BRK induces a SMAD4-dependent suppression of tumor suppressor FRK potentially resulting in the stimulation of EMT and, potentially, metastasis (Fig. 6H).

DISCUSSION

The cellular role of TGF-β/SMAD signaling pathway is a paradox in cancer. On one hand, *SMAD4*-deficient $Kras^{G12D}$ pancreatic mouse models showed the rapid development of pancreatic tumors (*27*), while restoration of SMAD4 induced apoptosis (*27*) and inhibited tumorigenesis in Smad4-defective cancer cells (*28*). On the other hand, knockdown of SMAD4 significantly reduced liver tumorigenesis in mice (*29*). The molecular mechanism of this duality is yet to be solved. Further, it was thought that ubiquitination, but not phosphorylation, may play a role in the regulation of SMAD4 function (*30*). Our current study demonstrates that activated BRK phosphorylates SMAD4 and regulates its stability.

In this study, we have shown that (i) activated BRK regulates TGF-β/SMAD signaling by interacting with SMAD2/3 and SMAD4; however, SMAD4 is the preferred target of BRK, as shown by the results of competitive binding (Fig. 2); (ii) activated BRK phosphorylates SMAD4 on tyrosine-353 and tyrosine-412 (Fig. 3); (iii) phosphorylated SMAD4 is the target of ubiquitin/deubiquitin ligases and is degraded by the ubiquitin-proteasome pathway (Fig. 5); (iv) the phosphorylation-regulated degradation of SMAD4 correlates well with the observation that BRK and SMAD4 show inverse expression patterns at the protein levels in breast cancer cells and tumors (Fig. 4); and (v) activated BRK modulates SMAD4 to suppress the tumor suppressor FRK, reduces the interaction of SMAD4 with cell adhesion molecules, and induces EMT (Fig. 6). Our study provides experimental evidence that the BRK kinase degrades SMAD4 to suppress tumor suppressor FRK and up-regulate EMT markers SNAIL and SLUG.

BRK is expressed in most of the cancer types. Although the expression of BRK is ubiquitous in most breast cancer cells and tumors, activated BRK was only detected in the plasma of breast tumors (*17*). Thus, in this study, we focused on characterizing activated BRK and its role in signal transduction pathways. A kinome array (*11*) was used to uncover the signal transduction pathways regulated by activated BRK in cancer and normal cells. Ectopically expressed activated BRK regulates the TGF-β/SMAD signaling pathways by interacting with SMAD2/3 and SMAD4. However, SMAD4 outcompetes both SMAD2 and SMAD3 in a binding assay for activated BRK. The BRK modular SH3 domain mediates its protein-protein interactions to regulate signaling (*31*). Notably, the SMAD4 activation domain is proline rich and contains the Pro-X-X-Pro motif (*32*), which is the recognition site for the SH3 domain (*33*). However, our domain truncation data indicate that activated BRK interacts with an MH1 domain of SMAD4, which does not contain the SH3 recognition motif, suggesting that the Pro-X-X-Pro motif might be dispensable for SH3-mediated protein-protein interactions.

Dupont *et al.* (*34*) previously found that a cycle of ubiquitination and deubiquitination regulates the function and protein-protein interaction of SMAD4: Ecto/TIF1γ-mediated monoubiquitination disassembles SMAD4 from the SMAD complex, while deubiquitination by FAM/USP9x allows SMAD4 to return to SMAD signaling pool. Our MudPIT-proteomics data revealed that BRK-phosphorylated SMAD4 interacts with several ubiquitin and deubiquitin ligases such as HERC2, RNF138 (ubiquitin ligases), and USP32, USP7, and USP9X (deubiquitinases). When phosphorylated by activated BRK, SMAD4 becomes a target of ubiquitin ligases (HERC2 and RNF138), which accelerates its degradation by the ubiquitin-proteasome pathway. Recently, SMAD4 has been shown to phosphorylate and degraded (on Thr^{277}) by glycogen synthase kinase 3 (*35*). However, phosphorylated SMAD4 also becomes a target of deubiquitin ligases (USP32, USP7, and USP9X). Deubiquitin ligase USP9X shows a stronger affinity for tyrosine phosphorylated SMAD4 than non-phosphorylated SMAD4. In addition, our evidence reveals that BRK or other protein tyrosine kinases [since protein tyrosine kinase are functionally redundant (*36*)] mediates phosphorylation of SMAD4, which is required for SMAD complexes to interact with chromatin remodelers such as SWI/SNF ((SWItch/Sucrose Non-Fermentable)), mediator, histone acetyltransferesase, or SIN3/histone deacetylase complexes for gene regulation (*28*, *37*). Notably, in our future study, we opt to explore the impact of SMAD4-chromatin remodeler complexes interaction on gene expression in normal and cancer cells.

Complete loss or mutation in SMAD4 has been reported in several cancer types, including pancreatic, cholangiocarcinoma, and colorectal cancer (*28*). In addition, SMAD4 protein levels decline concurrently with the cumulative malignancy of the tumor cells (*38*). Our data demonstrate differential expression of SMAD4 and BRK in a panel of breast cancer cell lines. An inverse pattern of SMAD4 and BRK protein levels was noticed in $HER2^{+}$ (HCC1428 and SKBR3) and TNBC (MDA-MB-231, BT20, Hs578T, BT549, and HCC1954) cells but not ER^{+} cells (T47D, MCF7, and BT474). However, there are no discrepancies in the expression of *SMAD4* and *BRK* at the mRNA level in those cell lines, indicating a post-translational mechanism of regulation of SMAD4. We also found that the inversely correlated pattern of expression between SMAD4 and BRK in patients' breast tumor tissues. In agreement with what is observed in TNBC cells, patients' breast tumor samples also show higher levels of the BRK protein in comparison to SMAD4. Furthermore, cells stably expressing activated BRK show a marked suppression of SMAD4 protein levels. We confirmed that p21, a known downstream target of SMAD4 (*28*, *37*), is suppressed in these cell lines expressing activated BRK. However, SMAD4 was not restored or up-regulated in MCF7 cells where BRK was knocked down. This suggests that SMAD4 escapes being targeted for proteasomal degradation, which could be due to a mutation or posttranslational modification of SMAD4 or inactivation of BRK in MCF7 cells.

The growth inhibitory signals of TGF-β/Smad4 signaling in early stages of carcinogenesis are well established. In particular, the involvement of SMAD4 in the EMT process and in cancer progression in later stages of carcinogenesis is largely unclear (*39*). Moreover, the function of SMAD4 is mostly contextual. Our data indicate that SMAD4 binds in the promoter region and promote FRK expression. However, in the presence of activated BRK, *FRK* expression is repressed in TNBC cells. Overexpression of SMAD4 restores the BRK-induced suppression of FRK level in the TNBC cells stably expressing BRK. Previous studies have shown that the expression of *SNAIL* is up-regulated in FRK–knocked down breast cancer cells (*25*). We observed that activated BRK induces *SLUG* and *SNAIL* expression, while overexpression of FRK significantly suppresses the mesenchymal marker *SLUG*, suggesting an FRK-dependent mechanism for BRK-induced promotion of EMT.

In summary, we provide additional evidence to counter the long-standing idea that SMAD4 is not regulated by phosphorylation. We have found that activated BRK competitively binds and phosphorylates SMAD4 and regulates TGF-β/SMAD signaling pathways. Phosphorylated SMAD4 becomes a target of ubiquitin ligases subsequently degraded through the ubiquitin-proteasome system leading the suppression of tumor suppressor FRK. Activated BRK also reduces cell adhesion ability and induces EMT in a SMAD4-dependent

manner. Thus, our data suggest that combination therapies targeting activated BRK signaling may be beneficial in the treatment of SMAD4-repressed cancers.

MATERIAL AND METHODS

Antibodies and reagents

The following antibodies were obtained from Santa Cruz Biotechnology (Santa Cruz, CA, USA): anti-BRK (sc-916 and sc-1188), antiphosphotyrosine PY20 (sc-508), anti-SMAD2/3/4, antitubulin (sc-9104), anti-GFP (sc-8334), and anti–β-actin (sc-130300). Anti–α-tubulin mouse monoclonal (T9026) antibody was purchased from Sigma-Aldrich (St. Louis, MO). Anti-Halo rabbit polyclonal antibody (G9281) and Magne HaloTag magnetic affinity beads were purchased from Promega (Madison, WI). Proteasome inhibitor MG132 was obtained from Sigma-Aldrich (St. Louis, MO).

Cell cultures

MCF10A, MCF12F, MDA-MB-231, BT20, HCC1428, SKBR3, Hs578T, T47D, BT549, MCF7, BT474, HCC1954, and HEK293 cells were purchased from and cultured according to the American Type Culture Collection (Manassas, VA, USA).

Construction of expression plasmids in human cells

The pGFP-C1-Smad2, pGFP-C1-Smad3, and pGFP-C1-Smad4 plasmids were a gift from C. Hill, Cancer Research UK. SMAD4 and BRK-YF were subcloned by inserting PCR products (containing SgfI and PmeI restriction sites) to generate pcDNA5-Halo-SMAD4 and pcDNA5-Halo-BRK-YF. Vectors expressing Halo-pcDNA5-Halo-SMAD4_1-140, pcDNA5-Halo-SMAD4_1-320, pcDNA5-Halo-SMAD4_140-320, pcDNA5-Halo-SMAD4_320-552, and pcDNA5-Halo-SMAD4_140-552 were constructed by inserting PCR products between the SgfI and PmeI restriction sites. We further subcloned SMAD4 into pcDNA5/FRT/TO vector (a gift from the Conaway Lab at Stowers Institute) using Gibson Assembly Cloning Kit [New England Biotechnologies (NEB)]. Human SMAD4 double mutant (Tyr^{353} Phe and Tyr^{412} Phe) was obtained using PCR and Gibson Assembly Cloning Kit (NEB). All plasmid constructs were confirmed by sequencing. The primers were used for cloning, and PCR were listed in table S3.

Generation of stable cell lines

The construction of cell lines stably expressing GFP-BRK-YF has been previously described (*2*). Amphotropic HEK293-derived Phoenix packaging cells were used to package pBabe-puro retroviral system. For retrovirus production, packaging cells were cultured in Dulbecco's modified Eagle's medium supplemented with 10% bovine calf serum. Transfection with 1% PEI (Polysciences Inc.) was conducted with 10 μg of retroviral DNA in 60 μl of 1% polyethylenimine plus 430 μl of 0.15 M NaCl for the 100-mm culture plates. After 24 and 48 hours, the virus-containing supernatant was collected and filtered through 0.45-μm syringe filter and aliquoted and stored at −80°C. To infect MCF10A, MDA-MB-231, and HEK293 cells, virus-containing supernatant was supplemented with bovine calf serum and polybrene (Sigma-Aldrich, St. Louis, MO) and overlaid on the cells. After overnight incubation, the viral supernatant was replaced with fresh culture medium. Pools of GFP-BRK-YF–expressing cells were selected with puromycin (Sigma-Aldrich). Expression of GFP-tagged BRK-YF was detected after 48 to 72 hours of infection by fluorescence microscopy. To produce stable BRK knockdown cell lines, we used BRK-expressing MCF7 parental cell lines. This knockdown experiment was performed according to the manufacturer's protocol using shRNA lentiviral vector plasmids from Santa Cruz Biotechnology. The shRNA plasmids generally consisted of a pool of three to five lentiviral vector plasmids, each encoding target-specific 19- to 25-nt shRNAs designed to knockdown gene expression. As controls, MCF7 cells were infected with a control shRNA and a GFP-control plasmid for transfection efficiency. Transfected cells were selected using puromycin (Sigma-Aldrich).

Kinome array

High-throughput kinome assay was performed according to the published protocol (*11*). Briefly, the MDA-MB-231, MCF10A, and HEK293 cells stably expressing GFP-BRK-YF were cultured to ~80% confluency in 10-cm culture plates. The cells were harvested and lysed with 100 μl of lysis buffer [20 mM tris-HCl (pH 7.5), 150 mM NaCl, 1 mM EDTA, 1 mM EGTA, 1% Triton X-100, 2.5 mM sodium pyrophosphate, 1 mM Na_3VO_4, 1 mM NaF, aprotinin (1 g/ml), leupeptin (1 μg/ml), and 1 mM phenylmethylsulphonyl fluoride (PMSF)] and incubated on ice for 10 min, followed by centrifugation at maximum speed in a microcentrifuge for 10 min at 4°C. A 70-μl aliquot of clear cells lysate was mixed with 10 μl of activation mix [50% glycerol, 50 μM adenosine 5′-triphosphate (ATP), 60 mM $MgCl_2$, 0.05% (v/v) Brij-35, bovine serum albumin (BSA; 0.25 mg/ml)] and incubated on the peptide array in a humidity chamber for 2 hours at 37°C. Arrays were then washed with phosphate-buffered saline (PBS) containing 1% Triton X-100. Slides were submerged in phosphospecific fluorescent ProQ Diamond Phosphoprotein Stain (Invitrogen) with agitation for 1 hour. Arrays were then washed three times in destain containing 20% acetonitrile (EMD Biosciences, VWR distributor, Mississauga, ON) and 50 mM sodium acetate (Sigma-Aldrich) at pH 4.0 for 10 min. A final wash was performed with distilled deionized H_2O. Arrays were air dried for 20 min and then centrifuged at 3009*g* for 2 min to remove any remaining moisture from the array. Arrays were analyzed using a GenePix Professional 4200A microarray scanner (MDS Analytical Technologies, Toronto, ON, Canada) at 532 to 560 nm with a 580-nm filter to detect dye fluorescence. Images were collected using the GenePix 6.0 software (MDS) and the spot intensity signal collected as the mean of pixel intensity using local feature background intensity background calculation with the default scanner saturation level. Data were processed using the PIIKA2 platform (http://saphire.usask.ca/saphire/piika/).

Preparation of cell lysates

Confluent or subconfluent cells were harvested and washed with ice-cold PBS (twice). The whole procedures were carried out at 4°C (on ice) unless specified otherwise. Cells were resuspended in freshly prepared lysis buffer [20 mM tris (pH 7.5), 1% Triton X-100, 150 mM NaCl, and protease inhibitors aprotinin (5 mg/liter) and 0.1 mM PMSF] and kept on ice for 30 min, followed by centrifugation at 14,000 rpm for 15 min at 4°C. Cells were directly lysed in SDS sample buffer [50 mM tris-HCl (pH 6.8), 2% SDS, 0.1% bromophenol blue, and 10% glycerol] to obtain total cell lysates.

Live-cell imaging

HEK293T cells were seeded onto glass-bottom culture dishes (MatTek, Ashland, MA) and transiently transfected with the SNAP-Flag-BRK and Halo-SMAD4 constructs. Affinity-tagged proteins were fluorescently labeled during growth, either with Halo-Tag TMRDirect ligand (Promega) or SNAP-Cell 505-Star (NEB) or with both ligands

according to the manufacturer's instructions. Images were taken with a ZEISS LSM 780 confocal microscope with argon laser excitation at 573 to 687 nm for TMRDirect and 499 to 526 nm for SNAP-Cell 505-Star. To limit photobleaching, exposure time and laser power were adjusted to enhance image quality. An alternating excitation mode was adopted to eliminate cross-talk between color channels. HaloTag-SMAD4 or SNAP-Tag BRK-YF were ectopically expressed in HEK293T cells and plated at 20% confluency onto glass-bottom MatTek culture dishes (35 mm, no. 2, 14-mm-diameter glass). To label Halo-SMAD4 proteins, the HaloTag TMRDirect ligand was added in a final concentration of 100 nM and incubated the cells overnight. In addition, the SNAP-Cell 505 ligands were added directly to the cells to label SNAP-Tag BRK-YF in a final concentration of 5 μM and incubated the cells for 1 hour at 37°C in 5% CO_2. For colocalization, Halo-SMAD4 and SNAP-Flag-BRK-YF constructs were cotransfected into HEK293T cells, and the cells were labeled as indicated above. The cultured media were replaced with OptiMEM to remove background fluorescence before imaging. Cells were stained with Hoechst dye to mark nuclei for 30 min before imaging.

Immunocytochemistry of BRK and SMAD4

MCF7 cells were cultured on MatTek plates before fixation with 4% paraformaldehyde (PFA) and permeabilized with permeabilizing buffer (0.5% Triton X-100) for 15 min. The permeabilized cells incubated in Odyssey blocking buffer for 1 hour. Then, cells were washed and incubated with monoclonal rabbit anti-BRK (1:100) and monoclonal mouse anti-SMAD4 (1:100) antibodies at room temperature for 2 hours, followed by incubation with goat anti-rabbit Alexa Fluor 488 and donkey anti-mouse Alexa Fluor 594 conjugated secondary antibody at room temperature for 1 hour. Immunostained cells were analyzed using a ZEISS LSM 700 confocal microscope with argon laser excitation at 488 nm (green), 561 nm (red), and 405 nm (blue). To remove any background, fluorescence cells were washed four times with TBST (tris-buffered saline and Tween 20) before imaging. Cells were stained with Hoechst dye to mark nuclei for 30 min before imaging.

Halo affinity purification of SMAD4 for proteomic analysis

HEK293T cells (1×10^7) were seeded into 15-cm tissue cultures plates for 24 hours, and then, DNA constructs encoding Halo or SNAP tagged genes of interest were transfected using Lipofectamine LTX (Thermo Fisher Scientific). Forty-eight hours after transfection, cells were harvested and washed twice with ice-cold PBS. The ice-cold PBS washed cells were resuspended in 300 μl of mammalian cell lysis buffer (Promega) containing 50 mM tris-HCl (pH 7.5), 150 mM NaCl, 1% Triton X-100, 0.1% sodium deoxycholate, 0.1 mM benzamidine HCl, 55 μM phenanthroline, 1 mM PMSF, 10 μM bestatin, 5 μM pepstatin A, and 20 μM leupeptin. Next, the cells were raptured by passing through a 26-gauge needle five to seven times, followed by centrifugation at 21,000*g* for 30 min at 4°C. The resulting 300 μl of cell extracts were collected into a new tube and diluted with 700 μl of tris-buffered saline [50 mM tris-HCl (pH 7.4), 137 mM NaCl, and 2.7 mM KCl]. To remove insoluble materials, the diluted cell extracts were further centrifuged at 21,000*g* for 10 min at 4°C. Next, 1000 μl of cell extracts were incubated with magnetic beads prepared from 100 μl of Magne HaloTag slurry for overnight at 4°C. Beads were washed four times (750 μl of buffer per wash) with wash buffer [50 mM tris-HCl (pH 7.4), 137 mM NaCl, 2.7 mM KCl, and 0.05% NP-40] before elution. Proteins were eluted using elution buffer containing 50 mM tris-HCl (pH 8.0), 0.5 mM EDTA, 0.005 mM dithiothreitol (DTT), and 2 U of AcTEV Protease (Thermo Fisher Scientific) for 2 hours at room temperature. The eluate was further passed through a Micro Bio-Spin column (Bio-Rad, Hercules, CA) to remove any residual particles of beads before proteomic analysis.

MudPIT analysis for identification of SMAD4-associated proteins and protein complexes

MudPIT analysis for protein complexes identification was previously described in detail by Banks *et al.* (*21*). Briefly, trichloroacetic acid precipitated purified proteins were proteolytically digested with endoproteinase Lys-C, followed by trypsin digestion, overnight at 37°C. A 10-step MudPIT separation approach was applied, and digested peptides were injected directly into a linear ion trap mass spectrometer, where spectra were collected and identified. Peptide mass spectra were analyzed using the ProLuCID and DTASelect algorithms. Next, we used Contrast and NSAF7 software to rank the putative affinity-purified proteins according to their distributed normalized spectral abundance values. We then used QSPEC software to identify enriched proteins in experimental samples compared to control samples. The Benjamini-Hochberg statistical method was used to calculate false discovery rates from QSPEC parameters suitable for multiple comparisons. Each of the experiments was repeated at least twice unless otherwise stated. All raw mass spectrometry runs are available, as described in table S3.

In vitro kinase assay

In vitro kinase assays were performed using 20 μl of affinity-purified Flag-BRK-YF and a 10-μl volume of affinity-purified substrate (SMAD4) in a reaction volume of 50 μl, comprising 20 μl of kinase buffer [25 mM tris-HCl (pH 7.5), 5 mM β-glycerophosphate, 2 mM DTT, 0.1 mM Na_3VO_4, and 10 mM $MgCl_2$; kinase buffer (10×) #9802, Cell Signaling Technology] with or without 200 μM ATP. The reaction was carried out at 30°C for 30 min and terminated by the addition of Laemmli sample buffer. The samples were then boiled for 10 min and resolved via SDS-PAGE.

RNA isolation and real-time PCR

Total RNA was isolated from MDA-MB-231 cells using RNeasy Plus Mini Kit (QIAGEN, Mississauga ON). Total RNA (1.0 μg) was used to synthesize complementary DNA (cDNA) using Bio-Rad Iscript cDNA Synthesis Kit (Bio-Rad, USA). TaqMan probes Hs00176619_m1, Hs00950344-m1, Hs 00195591_m1, and Hs02758991-g1 were used to quantify the expression of FRK, SLUG, SNAIL, and glyceraldehyde-3-phosphate dehydrogenase, as recommended by the manufacturer (Life Technologies, Burlington, ON, Canada). Briefly, 0.6 μl of cDNA, 0.5 μl of probes for each target and housekeeping genes, and 5 μl of TaqMan(R) Master Mix were added in each well. Distilled H_2O was added in each well to make the volume of 10 μl. Probes for target genes and housekeeping genes were labeled with FAM and VIC dyes, respectively. The expression of both genes was measured within the same well using an Applied Biosystems, Step One Plus qRT-PCR machine (Life Technologies, Burlington, ON, Canada). In addition, total RNA was also prepared from the whole cell extract using Direct-zolTM RNA Miniprep plus kits (Zymo Research, Irvine, CA) according to the manufacturer's instructions. Residual DNA was removed using deoxyribonuclease I. cDNA was synthesized using iScript Reverse Transcription Supermix (Bio-Rad), and the resulting cDNA was analyzed by qPCR using a MyiQ real-time

detection system (Bio-Rad). The primers were used for PCR are listed in table S3.

Ubiquitination assay under denaturing conditions

HEK293 cells were transfected in combination of Halo-SMAD4, HA-tagged ubiquitin, and/or SNAP-Flag-BRK-YF, and the cells were treated with 10 μM MG132 for 6 hours. Denatured cell extracts were prepared using denaturing buffer containing 1% SDS, 50 mM tris-HCl (pH 7.5), 150 mM NaCl, 1% Triton X-100, 0.1% sodium deoxycholate, 0.1 mM benzamidine HCl, 55 μM phenanthroline, 10 μM bestatin, 20 μM leupeptin, 5 μM pepstatin A, and 1 mM PMSF. Then, the cell lysates were and boiled for 10 min before incubation with primary mouse anti-SMAD4 antibody, followed by Dynabeads Protein G (Invitrogen) magnetic beads conjugation and immunoblotting with anti-HA antibody to detect ubiquitinated SMAD4.

Luciferase reporter assays

FRK promoter and SMAD4 plasmids were cotransfected in HEK293 cells using ViaFect (Promega Corporation, Madison, WI) according to the manufacturer's guidelines. Briefly, 125,000 HEK293 cells were seeded with 500 μl of fresh media in each well. The HEK293 cells were cotransfected with FRK promoter (495 ng; firefly luciferase) along with phRL-TK (5 ng; *Renilla* luciferase) as an internal control. Forty eight hours after transfection, cells were harvested, and luciferase activity was measured using the Dual-Luciferase Assay System with the GloMax 96 Microplate Luminometer (Promega Corporation). To examine the impact of SMAD4 on the *FRK* promoter, cells were cotransfected with GFP-SMAD4 plasmid (250 ng) and *FRK* reporters (245 ng), while control cells were cotransfected with FRK promoter construct and an empty vector (pCDNA3, 245 ng per well) and 5 ng of phRL-TK plasmids as an internal control in each well (Invitrogen, Canada).

Chromatin immunoprecipitation

ChIP was performed as described (*40*). Briefly, cells were cross-linked with 1% formaldehyde for 20 min before being sonicated using output power 3 (9-W power) for 10 cycles. Before the immunoprecipitation, Dynabeads Protein G (Invitrogen) magnetic beads were washed and coupled to 10 μg of anti-SMAD4 (sc-7966, Santa Cruz Biotechnology), and normal mouse immunoglobulin G (IgG) (sc-2025, Santa Cruz Biotechnology). Cell lysates were incubated with SMAD4 and IgG-conjugated magnetic beads for overnight at 4°C. Immunoprecipitated lysates were treated with proteinase K and incubated for overnight at 65°C before the DNA being extracted.

ChIP-qPCR

To determine whether SMAD4 binds to FRK promoter regions, we performed anti-SMAD4 and anti-IgG (control) ChIP using chromatin from MCF7 cells. Immunoprecipitation and input samples were analyzed by qPCR using PerfeCTa SYBR Green FastMix Low ROX (Quantabio) in a QantStudio 7 Flex-Thermal Cycler (Life Technologies–Applied Biosystems). PCR primers were used to amplify the regions at the FRK promoter. Transcription start sites and transcriptionally inactive genomic region are listed in table S3. Enrichment as a percentage of the input was calculated for each ChIP sample using the formula: $100 * 2\text{^}[C_t\text{Input} - \log_2(800/30) - C_t\text{ IP}]$, where 800/30 is the input dilution factor. For each ChIP, SMAD4 enrichment (ChIP/input) in the promoter was normalized to the average of the ChIP/input values from a transcriptionally inactive genomic region. In this experiment, C_t values of two biological replicates of at least three technical replicates were used for the analysis.

Cell adhesion assay

Ninety-six–well plates were coated with either fibronectin or collagen I for an hour at 37°C, followed by an hour of incubation with 0.5% BSA-containing blocking buffer. HEK293 or MCF10A cells were seeded at a density of 4×10^5, and cells were allowed to attach for 45 min at 37°C. The cells were washed three times with 0.1% BSA-containing culture media, and then, the cells were fixed with 4% PFA. Next, the cells were stained with crystal violet for 10 min. After staining, the cells were washed 10 times with distilled water. Cells were air-dried for an hour and solubilized with 2% SDS on an agitator. The absorbance of each well was measured at 550 nm to quantify the adhesion properties of cells.

Statistical analysis

For multiple comparisons (qPCR and adhesion assay), one-way analysis of variance (ANOVA) followed by a post hoc Newman-Keuls test was used using GraphPad Prism version 5.04 (GraphPad Software, San Diego, CA, USA; www.graphpad.com). The results are presented as the means ± SD, $n \geq 3$, unless otherwise stated. $P \leq 0.05$ was considered statistically significant.

SUPPLEMENTARY MATERIALS

Supplementary material for this article is available at http://advances.sciencemag.org/cgi/content/full/5/10/eaaw3113/DC1

Fig. S1. The kinase activity of BRK and regulated signaling pathways.
Fig. S2. Identification of Halo-SMAD4–associated proteins.
Fig. S3. Activated BRK phosphorylates tyrosine-353 and tyrosine-412 on SMAD4.
Fig. S4. BRK and SMAD4 mRNA and protein expression in different cells.
Fig. S5. Halo-SMAD4/Halo-SMAD4 Y353F– and Halo-SMAD4 Y412F–associated proteins in the presence or absence of SF-BRK-YF and their ubiquitination.
Fig. S6. Gene ontology analyses for cellular components represented in the proteins associated with Halo-SMAD4 and phosphorylated Halo-SMAD4.
Fig. S7. FRK-dependent regulation of EMT markers.
Table S1. Differential protein interaction of Halo-SMAD4 in the presence of SNAP-F-BRK-WT or SNAP-F-BRK-YF (QSPEC $\log_2$ fold change, ≥1; QSPEC false discovery rate, ≤0.05).
Table S2. Phosphorylation sites on SMAD4 detected by MudPIT analyses of in presence or absence of BRK-YF.
Table S3. Gene ontology analysis for cellular component of Halo-SMAD4 in the presence of SNAP-F-BRK-WT or SNAP-F-BRK-YF in ClueGO FDR_0.05; Zscore_3: Tab: 3. Primers: Tab: 3. References (*41*, *42*)

View/request a protocol for this paper from *Bio-protocol*.

REFERENCES AND NOTES

1. J. Jiang, F. Gui, Z. He, L. Li, Y. Li, S. Li, X. Wu, Z. Deng, X. Sun, X. Huang, W. Huang, S. Han, T. Zhang, Z. Wang, B. Jiao, S. Song, H. Wang, L. Chen, D. Zhou, Q. Liu, R. Ren, J. Zhang, X. Deng, Targeting BRK-positive breast cancers with small-molecule kinase inhibitors. *Cancer Res.* **77**, 175–186 (2017).
2. S. Miah, A. Martin, K. E. Lukong, Constitutive activation of breast tumor kinase accelerates cell migration and tumor growth in vivo. *Oncogene* **1**, e11 (2012).
3. P. M. Brauer, A. L. Tyner, Building a better understanding of the intracellular tyrosine kinase PTK6 — BRK by BRK. *Biochim. Biophys. Acta.* **1806**, 66–73 (2010).
4. T. Kamalati, H. E. Jolin, M. J. Fry, M. R. Crompton, Expression of the BRK tyrosine kinase in mammary epithelial cells enhances the coupling of EGF signalling to PI 3-kinase and Akt, via erbB3 phosphorylation. *Oncogene* **19**, 5471–5476 (2000).
5. J. H. Ostrander, A. R. Daniel, K. Lofgren, C. G. Kleer, C. A. Lange, Breast tumor kinase (protein tyrosine kinase 6) regulates heregulin-induced activation of ERK5 and p38 MAP kinases in breast cancer cells. *Cancer Res.* **67**, 4199–4209 (2007).
6. H.-Y. Chen, C.-H. Shen, Y.-T. Tsai, F.-C. Lin, Y.-P. Huang, R.-H. Chen, Brk activates Rac1 and promotes cell migration and invasion by phosphorylating paxillin. *Mol. Cell. Biol.* **24**, 10558–10572 (2004).

7. B. Xiang, K. Chatti, H. Qiu, B. Lakshmi, A. Krasnitz, J. Hicks, M. Yu, W. T. Miller, S. K. Muthuswamy, Brk is coamplified with ErbB2 to promote proliferation in breast cancer. *Proc. Natl. Acad. Sci.* **105**, 12463–12468 (2008).
8. C. Fan, Y. Zhao, D. Liu, X. Zhang, E. Wang, Detection of Brk expression in non-small cell lung cancer: Clinicopathological relevance. *Tumour Biol.* **32**, 873–880 (2011).
9. R. E. Schmandt, M. Bennett, S. Clifford, A. Thornton, F. Jiang, R. R. Broaddus, C. C. Sun, K. H. Lu, A. K. Sood, D. M. Gershenson, The BRK tyrosine kinase is expressed in high-grade serous carcinoma of the ovary. *Cancer Biol. Ther.* **5**, 1136–1141 (2006).
10. H. Ono, M. D. Basson, H. Ito, PTK6 promotes cancer migration and invasion in pancreatic cancer cells dependent on ERK signaling. *PLOS ONE* **9**, e96060 (2014).
11. S. Jalal, R. Arsenault, A. A. Potter, L. A. Babiuk, P. J. Griebel, S. Napper, Genome to kinome: Species-specific peptide arrays for kinome analysis. *Sci. Signal.* **2**, pl1 (2009).
12. Y. E. Zhang, Mechanistic insight into contextual TGF-β signaling. *Curr. Opin. Cell Biol.* **51**, 1–7 (2018).
13. J. M. Kang, S. Park, S. J. Kim, H. Y. Hong, J. Jeong, H. S. Kim, S. J. Kim, CBL enhances breast tumor formation by inhibiting tumor suppressive activity of TGF-β signaling. *Oncogene* **31**, 5123–5131 (2012).
14. C. J. David, Y. H. Huang, M. Chen, J. Su, Y. Zou, N. Bardeesy, C. A. Iacobuzio-Donahue, J. Massagué, TGF-β tumor suppression through a lethal EMT. *Cell* **164**, 1015–1030 (2016).
15. K. Park, S. J. Kim, Y. J. Bang, J. G. Park, N. K. Kim, A. B. Roberts, M. B. Sporn, Genetic changes in the transforming growth factor beta (TGF-β) type II receptor gene in human gastric cancer cells: Correlation with sensitivity to growth inhibition by TGF-beta. *Proc. Natl. Acad. Sci. U.S.A.* **91**, 8772–8776 (1994).
16. C. Kandoth, M. D. McLellan, F. Vandin, K. Ye, B. Niu, C. Lu, M. Xie, Q. Zhang, J. F. McMichael, M. A. Wyczalkowski, M. D. M. Leiserson, C. A. Miller, J. S. Welch, M. J. Walter, M. C. Wendl, T. J. Ley, R. K. Wilson, B. J. Raphael, L. Ding, Mutational landscape and significance across 12 major cancer types. *Nature* **502**, 333–339 (2013).
17. M. Peng, R. Emmadi, Z. Wang, E. L. Wiley, P. H. Gann, S. A. Khan, N. Banerji, W. McDonald, S. Asztalos, T. N. Pham, D. A. Tonetti, A. L. Tyner, PTK6/BRK is expressed in the normal mammary gland and activated at the plasma membrane in breast tumors. *Oncotarget* **5**, 6038–6048 (2014).
18. N. Dhanasekaran, E. P. Reddy, Signaling by dual specificity kinases. *Oncogene* **17**, 1447–1455 (1998).
19. S. Tyanova, R. Albrechtsen, P. Kronqvist, J. Cox, M. Mann, T. Geiger, Proteomic maps of breast cancer subtypes. *Nat. Commun.* **7**, 10259 (2016).
20. A. Moustakas, D. Kardassis, Regulation of the human p21/WAF1/Cip1 promoter in hepatic cells by functional interactions between Sp1 and Smad family members. *Proc. Natl. Acad. Sci.* **95**, 6733–6738 (1998).
21. C. A. S. Banks, J. L. Thornton, C. G. Eubanks, M. K. Adams, S. Miah, G. Boanca, X. Liu, M. L. Katt, T. J. Parmely, L. Florens, M. P. Washburn, A structured workflow for mapping human Sin3 histone deacetylase complex interactions using Halo-MudPIT AP-MS. *Mol. Cell. Proteomics* **17**, 1432–1447 (2018).
22. G. A. Collins, A. L. Goldberg, The logic of the 26S proteasome. *Cell* **169**, 792–806 (2017).
23. S. Akhavantabasi, H. B. Akman, A. Sapmaz, J. Keller, E. M. Petty, A. E. Erson, *USP32* is an active, membrane-bound ubiquitin protease overexpressed in breast cancers. *Mamm. Genome* **21**, 388–397 (2010).
24. R. K. Goel, K. E. Lukong, Understanding the cellular roles of Fyn-related kinase (FRK): Implications in cancer biology. *Cancer Metastasis Rev.* **35**, 179–199 (2016).
25. Y. Ogunbolude, C. Dai, E. T. Bagu, R. K. Goel, S. Miah, J. MacAusland-Berg, C. Y. Ng, R. Chibbar, S. Napper, L. Raptis, F. Vizeacoumar, F. Vizeacoumar, K. Bonham, K. E. Lukong, FRK inhibits breast cancer cell migration and invasion by suppressing epithelial-mesenchymal transition. *Oncotarget* **8**, 113034–113065 (2017).
26. J. Massagué, J. Seoane, D. Wotton, Smad transcription factors. *Genes Dev.* **19**, 2783–2810 (2005).
27. N. Bardeesy, K. H. Cheng, J. H. Berger, G. C. Chu, J. Pahler, P. Olson, A. F. Hezel, J. Horner, G. Y. Lauwers, D. Hanahan, R. A. DePinho, Smad4 is dispensable for normal pancreas development yet critical in progression and tumor biology of pancreas cancer. *Genes Dev.* **20**, 3130–3146 (2006).
28. M. Zhao, L. Mishra, C.-X. Deng, The role of TGF-β/SMAD4 signaling in cancer. *Int. J. Biol. Sci.* **14**, 111–123 (2018).
29. H. Moon, H. L. Ju, S. I. Chung, K. J. Cho, J. W. Eun, S. W. Nam, K. H. Han, D. F. Calvisi, S. W. Ro, Transforming growth factor-β promotes liver tumorigenesis in mice via up-regulation of snail. *Gastroenterology* **153**, 1378–1391 (2017).
30. C. Le Goff, C. Mahaut, A. Abhyankar, W. Le Goff, V. Serre, A. Afenjar, A. Destrée, M. di Rocco, D. Héron, S. Jacquemont, S. Marlin, M. Simon, J. Tolmie, A. Verloes, J. L. Casanova, A. Munnich, V. Cormier-Daire, Mutations at a single codon in Mad homology 2 domain of SMAD4 cause Myhre syndrome. *Nat. Genet.* **44**, 85–88 (2012).
31. B. J. Mayer, The discovery of modular binding domains: Building blocks of cell signalling. *Nat. Rev. Mol. Cell Biol.* **16**, 691–698 (2015).
32. X.-H. Feng, Y. Zhang, R.-Y. Wu, R. Derynck, The tumor suppressor Smad4/DPC4 and transcriptional adaptor CBP/p300 are coactivators for Smad3 in TGF-β-induced transcriptional activation. *Genes Dev.* **12**, 2153–2163 (1998).
33. R. Ren, B. J. Mayer, P. Cicchetti, D. Baltimore, Identification of a ten-amino acid proline-rich SH3 binding site. *Science* **259**, 1157–1161 (1993).
34. S. Dupont, A. Mamidi, M. Cordenonsi, M. Montagner, L. Zacchigna, M. Adorno, G. Martello, M. J. Stinchfield, S. Soligo, L. Morsut, M. Inui, S. Moro, N. Modena, F. Argenton, S. J. Newfeld, S. Piccolo, FAM/USP9x, a deubiquitinating enzyme essential for TGFβ signaling, controls Smad4 monoubiquitination. *Cell* **136**, 123–135 (2009).
35. H. Demagny, T. Araki, E. M. De Robertis, The tumor suppressor Smad4/DPC4 is regulated by phosphorylations that integrate FGF, Wnt, and TGF-β signaling. *Cell Rep.* **9**, 688–700 (2014).
36. A. Y. Tsygankov, Non-receptor protein tyrosine kinases. *Front. Biosci.* **8**, s595–s635 (2003).
37. J. Massagué, TGFβ signalling in context. *Nat. Rev. Mol. Cell Biol.* **13**, 616–630 (2012).
38. C. H. Stuelten, M. B. Buck, J. Dippon, A. B. Roberts, P. Fritz, C. Knabbe, Smad4-expression is decreased in breast cancer tissues: A retrospective study. *BMC Cancer* **6**, 25 (2006).
39. P. M. Siegel, J. Massagué, Cytostatic and apoptotic actions of TGF-β in homeostasis and cancer. *Nat. Rev. Cancer* **3**, 807–820 (2003).
40. T. I. Lee, S. E. Johnstone, R. A. Young, Chromatin immunoprecipitation and microarray-based analysis of protein location. *Nat. Protoc.* **1**, 729–748 (2006).
41. G. Bindea, B. Mlecnik, H. Hackl, P. Charoentong, M. Tosolini, A. Kirilovsky, W. H. Fridman, F. Pagès, Z. Trajanoski, J. Galon, ClueGO: A Cytoscape plug-in to decipher functionally grouped gene ontology and pathway annotation networks. *Bioinformatics* **25**, 1091–1093 (2009).
42. P. Shannon, A. Markiel, O. Ozier, N. S. Baliga, J. T. Wang, D. Ramage, N. Amin, B. Schwikowski, T. Ideker, Cytoscape: A software environment for integrated models of biomolecular interaction networks. *Genome Res.* **13**, 2498–2504 (2003).

Acknowledgments: We thank S. E. Kong for insightful comments. We thank C. Hill, Cancer Research UK for SMAD2/3/4 plasmids. **Funding:** This work was supported by the Stowers Institute for Medical Research and the National Institute of General Medical Sciences of the NIH under award number RO1GM112639 to M.P.W. The content is solely the responsibility of the authors and does not necessarily represent the official views of the NIH. In addition, the work was supported by the 2017 College of Medicine Research Award (CoMRAD) offered by Office of the Vice Dean Research (OVDR) at the University of Saskatchewan, Saskatoon, Canada to K.E.L. and by the National Science and Engineering Research Council of Canada to S.N. **Author contributions:** S.M. conceptualized and interpreted all experiments. S.M., C.A.S.B., A.S., L.F., S.N., K.E.L., and M.P.W. designed experiments. S.M., C.A.S.B., Y.O., E.T.B., J.M.B., A.S., T.T.T., C.G.K., and G.D. performed experiments. S.M., C.A.S.B., E.T.B., A.S., L.F., T.T.T., G.D., G.H., M.S., S.N., L.F., K.E.L., and M.P.W. analyzed data and interpreted findings. K.E.L. and M.P.W. guided the research. S.M. wrote the manuscript with input from C.A.S.B., S.N., L.F., K.E.L., and M.P.W. **Competing interests:** The authors declare that they have no conflict of interest. **Data and materials availability:** All data needed to evaluate the conclusions in the paper are present in the paper and/or the Supplementary Materials. Data produced for this manuscript are available from the Stowers Original Data Repository at www.stowers.org/research/publications/LIBPB-1340. The mass spectrometry datasets were produced for this study are available from the Massive data repository (https://massive.ucsd.edu) using the identifiers listed in table S3. Additional data related to this paper may be requested from the authors.

Submitted 7 December 2018
Accepted 13 September 2019
Published 23 October 2019
10.1126/sciadv.aaw3113

Citation: S. Miah, C. A. S. Banks, Y. Ogunbolude, E. T. Bagu, J. M. Berg, A. Saraf, T. T. Tettey, G. Hattem, G. Dayebgadoh, C. G. Kempf, M. Sardiu, S. Napper, L. Florens, K. E. Lukong, M. P. Washburn, BRK phosphorylates SMAD4 for proteasomal degradation and inhibits tumor suppressor FRK to control SNAIL, SLUG, and metastatic potential. *Sci. Adv.* **5**, eaaw3113 (2019).

BRK phosphorylates SMAD4 for proteasomal degradation and inhibits tumor suppressor FRK to control SNAIL, SLUG, and metastatic potential

S. Miah, C. A. S. Banks, Y. Ogunbolude, E. T. Bagu, J. M. Berg, A. Saraf, T. T. Tettey, G. Hattem, G. Dayebgadoh, C. G. Kempf, M. Sardiu, S. Napper, L. Florens, K. E. Lukong and M. P. Washburn

Sci Adv **5** (10), eaaw3113.
DOI: 10.1126/sciadv.aaw3113